PLOS Pathogens

RESEARCH ARTICLE

Uukuniemi virus infection causes a pervasive remodelling of the RNA-binding proteome in tick cells

Alexandra Wilson[1,2‡], Wael Kamel[1‡], Kelsey Davies[1], Zaydah R. De Laurent[1], Rozeena Arif[1], Andrew T. Clarke[1], Lesley Bell-Sakyi[3], Douglas Lamont[4], Yana Demyanenko[5], Marko Noerenberg[1], Alain Kohl[1,6], Shabaz Mohammed[5,7,8], Alfredo Castello[1]*, Benjamin Brennan[1]*

1 Medical Research Council–University of Glasgow Centre for Virus Research, Glasgow, Scotland, United Kingdom, **2** Department of Experimental Biology, Faculty of Science, Masaryk University, Brno, Czech Republic, **3** Department of Infection Biology and Microbiomes, Institute of Infection, Veterinary and Ecological Sciences, University of Liverpool, Liverpool, United Kingdom, **4** FingerPrints Proteomics Facility, School of Life Sciences, University of Dundee, Dundee, Scotland, United Kingdom, **5** Rosalind Franklin Institute, Harwell Science and Innovation Campus, Oxford, Oxfordshire, United Kingdom, **6** Departments of Tropical Disease Biology and Vector Biology, Liverpool School of Tropical Medicine, Liverpool, United Kingdom, **7** Department of Chemistry, University of Oxford, Oxford, United Kingdom, **8** Department of Biochemistry, University of Oxford, Oxford, United Kingdom

‡ joint first authors
* ben.brennan@glasgow.ac.uk (BB); alfredo.castello@glasgow.ac.uk (AC)

Citation: Wilson A, Kamel W, Davies K, De Laurent ZR, Arif R, Clarke AT, et al. (2025) Uukuniemi virus infection causes a pervasive remodelling of the RNA-binding proteome in tick cells. PLoS Pathog 21(8): e1013393. https://doi.org/10.1371/journal.ppat.1013393

Editor: Kevin Maringer, Pirbright Institute, UNITED KINGDOM OF GREAT BRITAIN AND NORTHERN IRELAND

Received: January 8, 2025

Accepted: July 21, 2025

Published: August 4, 2025

Data availability statement: All data that support the findings of this study are openly available from Enlighten Research Data (http://dx.doi.org/10.5525/gla.researchdata.1983). The mass spectrometry proteomics data have been deposited to the ProteomeXchange Consortium

Abstract

Cellular RNA-binding proteins (RBPs) are pivotal for the viral lifecycle, mediating key host-virus interactions that promote or repress virus infection. While these interactions have been largely studied in the vertebrate host, no comprehensive analyses of protein-RNA interactions occurring in cells of arbovirus vectors, in particular ticks, have been performed to date. Here we systematically identified the responses of the RNA-binding proteome (RBPome) to infection with a prototype bunyavirus (Uukuniemi virus; UUKV) in tick cells and discovered changes in RNA-binding activity for 283 proteins. In an orthogonal approach, we analysed the composition of the viral ribonucleoprotein by immunoprecipitation of UUKV nucleocapsid protein (N) in infected cells. We found many tick RBPs that are regulated by UUKV infection and associate with viral nucleocapsid protein complexes, and we confirmed experimentally that they impact UUKV infection. This includes the tick homolog of topoisomerase 3B (TOP3B), a protein able to manipulate the topology of RNA, which particularly affected viral particle production. Our data thus reveals the first protein-RNA interaction map for infected tick cells.

via the PRIDE partner repository with the dataset identifier PXD059189. The R scripts used for analysis can be found in the Zenodo online repository (https://doi.org/10.5281/zenodo.15528292).

Funding: This research was funded by the University of Glasgow MVLS DTP (A.W.) and a Wellcome Trust/Royal Society Sir Henry Dale Fellowship (210462/Z/18/Z to B.B.). The facilities used in this study were funded by the UK Medical Research Council (MC_UU_00034/4, MC_UU_00034/8). L.B.S. was supported by the Wellcome Trust grant no. 223743/Z/21/Z. A.C. is funded by the European Research Council (ERC) Consolidator Grant 'vRNP-capture' 101001634 and the MRC grants MR/R021562/1 and MC_UU_00034/2. Y.D. and S.M. are funded by an EPSRC grant (V011359/1 (P)). A.K., was funded by the UK Medical Research Council (MC_UU_12014/8, MC_UU_00034/4). This research was funded in whole or in part by the Wellcome Trust. The funders had no role in study design, data collection and analysis, decision to publish, or preparation of the manuscript. The funders had no role in study design, data collection and analysis, decision to publish, or preparation of the manuscript.

Competing interests: The authors have declared that no competing interests exist.

Author summary

In host cells, RNA-binding proteins play essential roles in the life cycle of many viruses by influencing how viral RNA is processed, translated, replicated and assembled into virions. While these interactions have been extensively studied in mammalian hosts, much less is known about how their function in arthropod vectors, particularly ticks. In this study, we investigated how tick cell RNA-binding proteins respond to infection with a representative bunyavirus. We used a systematic approach to map the RNA-binding activity of proteins in tick cells and identified over 200 that are modulated during infection. In parallel, we isolated viral ribonucleoprotein complexes from infected cells to determine which of the regulated RNA-binding proteins physically associate with viral RNA and proteins. Several of these proteins regulated viral fitness, including a tick version of topoisomerase 3B that reduced viral particle production. Our findings provide the first comprehensive map of host protein–RNA interactions during viral infection in tick cells, offering new insight into the molecular interface between arboviruses and their vectors.

Introduction

Uukuvirus uukuniemiense is the prototypic virus within the genus *Uukuvirus* of the family *Phenuiviridae* that was first isolated from *Ixodes ricinus* ticks in Finland in 1964 [1]. Uukuniemi virus (UUKV; strain S-23) has been utilised as the prototype tickborne bunyavirus for several decades and has contributed to many aspects of bunyavirus research [2,3], such as the determination of the tri-segmented nature of bunyaviruses [4], the isolation of the first RNA-dependent RNA polymerase from a bunyavirus [5], the determination of the structural composition of the virion [6] and entry into mammalian cells [7–9]. Like other phenuiviruses, the genome of UUKV comprises three segments of negative or ambi-sense RNA, named small (S), medium (M) and large (L), which are deposited into the cytoplasm of infected cells as ribonucleoprotein (RNP) complexes encapsidated by the viral nucleocapsid (N) protein and associated with the viral RNA-dependent RNA polymerase (L protein). Both the N and L proteins can interact with and bind viral RNA, although currently it is unclear if this binding capability extends to cellular RNA [10,11]. The N protein has also been shown to interact with the L protein, the viral glycoproteins and a range of cellular proteins during infection [12,13]. The virus also encodes a non-structural protein (NSs) within the S segment that has been demonstrated to be a weak interferon antagonist [14]. However, unlike other phenuiviruses transmitted by mosquitoes or sandflies, the M segment of tickborne phenuiviruses only encodes the glycoprotein precursor and does not encode any other non-structural proteins [15].

Research into tickborne bunyaviruses has been heavily biased towards studies in vertebrate systems, primarily due to the expertise needed and expense of facilities associated with working with live ticks, and the lack of genomic data or molecular

reagents to conduct virus infection experiments within tick-derived cell lines. To date, over 70 cell lines have been developed from multiple tick species of medical and veterinary importance [16]. However, only within recent years have detailed whole tick genomes and the genome of an *Ixodes scapularis* cell line been sufficiently annotated to support studies into the molecular interactions of tickborne pathogens with host cells [17–19]. These tools have facilitated several groups to conduct proteomic, transcriptomic and genomic analyses of tick-derived cell lines [20–28]. However, no research has been carried out to determine the host proteins with pivotal roles in the lifecycle of a bunyavirus within tick cells.

Viruses, including those with a RNA based genome, have a limited coding capacity, and therefore cannot encode all the proteins required for a fully autonomous lifecycle, relying on host resources to replicate and spread. For example, viruses are fully dependent on the translation apparatus of the host cell to synthesise viral proteins. However, protein synthesis is just one of the many steps of viral RNA metabolism, and RNA-binding proteins (RBPs) are expected to additionally participate in RNA stability, replication and packaging of the viral RNA within the viral particles [29]. RBPs are also critical in the cellular defence against viruses. In vertebrates, RNA-binding sensors and effectors recognise molecular patterns that are specific to viral RNAs. In invertebrates, it is believed that the RNA interference (RNAi) pathway, which utilises many RBPs such as Dicer and Argonaute proteins, is the main effector of the antiviral response. However, whether other antiviral mechanisms involving RBPs exist in arthropods, as observed in vertebrates, remains unexplored. Despite the central roles that RNA plays in the viral lifecycle, the complement of host RBPs that participate in arboviral infection remain largely unknown, particularly for arthropod vectors such as ticks [30–33]. This has led to a dearth of information and insight as to why and how these important vectors can cause consequential diseases globally.

In this study, we utilise our proteome-wide approach called RNA interactome capture (RIC) to study the responses of the tick RNA-binding proteome (RBPome) of the *I. scapularis* cell line ISE6 to infection with UUKV [34,35]. We discovered that the tick RBPome is plastic and reconfigures in response to infection, with nearly three hundred proteins exhibiting either an increased or decreased RNA-binding activity. In addition, we conducted an orthogonal approach to isolate the viral ribonucleoproteins via immunoprecipitation of the UUKV N protein. Strikingly, we found 18 RBPs with virus-regulated RNA-binding activity that are also associated with the viral ribonucleoproteins. We validated our findings with dsRNA knockdowns in ISE6 cell cultures showing that the discovered RBPs do regulate virus infection. Initial characterisation of the selected candidates revealed a role for the protein ISCI010954 (TOP3B in vertebrates) in the production of infectious virus particles by facilitating the efficient packaging of UUKV RNAs into virions.

Results

Establishing comparative RNA interactome capture (cRIC) in tick cells

Earlier studies showed that virus infection causes a pervasive remodelling of the cellular RBPome in human cells [31,32,36]. Our goal was to determine whether such a phenomenon also occurs during infection of cells from the tick, and if so, whether it is biologically relevant. We adapted comparative RNA interactome capture to mock or UUKV-infected tick cells (Fig 1A) [34,37].

To determine which timepoint to utilise for this analysis, we conducted a viral growth curve to examine UUKV infection kinetics in ISE6 cells. Release of infectious virus was detected throughout the course of infection and progressively increased until the final time point at 12 days post infection (p.i.) (Fig 1B). In parallel, expression of the viral nucleocapsid protein (N) was monitored in infected cell lysates. UUKV N protein was detectable by Western blotting from 9 days p.i. (Fig 1C). There was a strong increase in UUKV N abundance and viral titre from 9 to 12 days p.i., which also implied active replication. UUKV-infected cell monolayers were also analysed by confocal microscopy through staining the monolayer for the presence of the UUKV N protein. This qualitative assessment (Fig 1D) provided assurance that most cells were infected (~80%) at the 9 days p.i. timepoint and confirmed its suitability for cRIC analysis (Fig 1D). Additionally, detection of UUKV N at this timepoint indicates its suitability for co-immunoprecipitation experiments to examine the UUKV N interactome and its connections with RBPome dynamics.

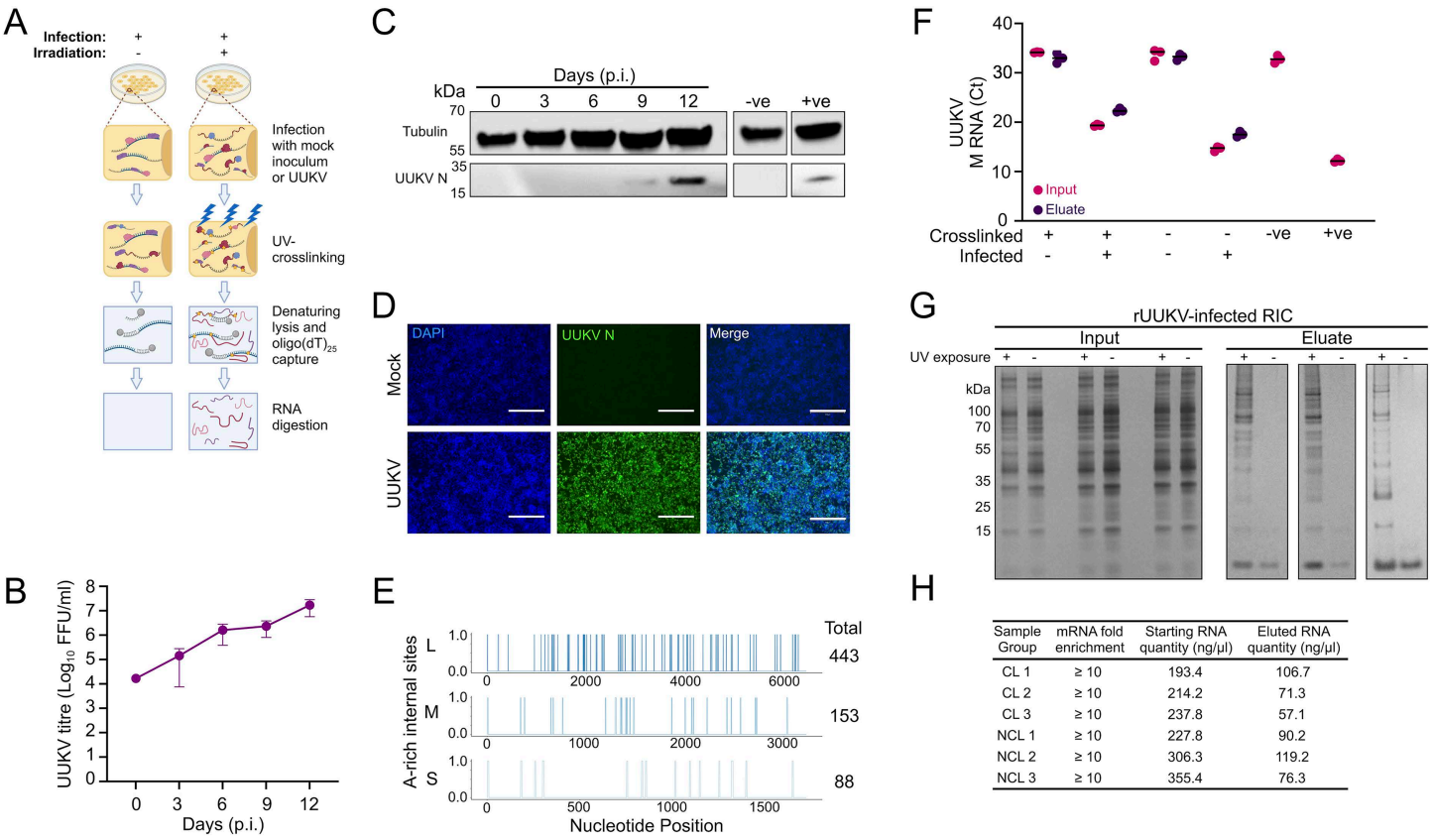

Fig 1. Preparation of mock and 5 MOI UUKV-infected RNA interactome capture (RIC) samples derived from ISE6 tick cell cultures. (A) Schematic showing the methodology of interactome capture utilising UV-crosslinking and oligo(dT)$_{25}$ capture beads. Created in BioRender. Brennan, B. (2025) https://BioRender.com/5ai6qjs. (B) Titre of UUKV in supernatant of infected ISE6 cells up to 12 days p.i. Data are plotted as the mean virus titre (FFU/ml) ± SD of n = 3 biological replicates. (C) Representative images of cell extracts from cell monolayers in (B) probed with anti-Tubulin, and anti-UUKV N antibodies. '-ve': mock-infected cell lysate; '+ve': sample known to be infected with UUKV derived from infected mammalian cells. (D) UUKV-infected ISE6 cell monolayers stained with DAPI (blue), and probed for UUKV N protein (green) at 9 days p.i. Cell monolayers were imaged using an EVOS microscope using a 10x objective. Scale bar is equal to 300 µm. (E) The poly(A) adjacent content of the UUKV genome segments. The involvement of each nucleotide in poly(A)/poly(A)-like sites is visualized. (F) Quantity of UUKV M RNA within input and eluate samples of ISE6 cell monolayers treated by RIC. (G) Proteins found in UUKV-infected ISE6 cells, derived from input or eluate RIC samples, visualised via silver staining. (H) Properties of RNA found within the samples described in (G). RT qPCR was performed against the 18S ribosomal RNA and eukaryotic elongation factor 1-alpha (*ELF1A*; mRNA used as a housekeeping gene) The ΔΔCT method was used to measure the quantity of 18S RNA normalized to *ELF1A* RNA levels. The mRNA fold enrichment in the elute compared to the input sample was calculated for each biological sample. Finally, the RNA quantities in the samples from (G) were measured via a Nanodrop spectrophotometer.

https://doi.org/10.1371/journal.ppat.1013393.g001

During initial infection, the ratio of viral RNA to cellular mRNA increases and this can lead to an interference with cellular mRNA production or stability [38,39]. To obtain a complete picture of the intracellular environment during UUKV infection of ISE6 cells, it was therefore important to assess whether the probes capture both cellular and viral RNA. This presents a problem, as bunyaviral genomic RNA or mRNAs are non-polyadenylated [40,41] and the oligo(dT)$_{25}$ capture beads used in cRIC exploit the interaction between the poly-A tail of mRNAs. Additionally, since UV crosslinking efficiency is low (typically peaking around 30%), with many RBPs crosslinking at 1% or less [42], probe hybridisation likely contributes significantly to RNA capture. UV-crosslinking induces covalent bonds between closely positioned nucleotides and amino acids with high specificity but low efficiency. For protein-coated RNAs such as the UUKV genomic RNA, only a subset of proteins would be covalently crosslinked. Denaturing lysis can then remove non-covalently bound proteins,

exposing protein-free RNA regions accessible to antisense probe hybridization. We analysed the genome of UUKV for the presence of 'poly-A like' regions, which we defined as a minimum of five sequential A nucleotides and any larger region containing a ≥ 80% A content. Our hypothesis was that oligo$(dT)_{25}$ capture beads would be able to capture the UUKV RNA by interacting with these 'poly-A like' regions, allowing the interactome capture to reflect both viral and cellular RNA within the infected cells. Our *in-silico* analysis revealed 88, 153 and 443 poly-A-like regions present within the UUKV S, M and L RNAs, respectively (Fig 1E). These results provided a basis for continuing with the UUKV-infected cRIC experimental protocol.

We next assessed the isolation of UUKV RNAs using RT-qPCR in cRIC eluates focusing on the M segment. UUKV RNAs were detected in all infected samples but not in the mock samples (Figs 1F and S1). These data confirmed that oligo$(dT)_{25}$ capture can isolate UUKV RNA transcripts; however, capture efficiency of individual viral RNA segments is dependent on the incidence of 'poly-A' like regions in the genome and overall viral RNA abundance in the input samples (Fig 1E and 1F). In parallel, cRIC inputs and eluates were quality controlled for RBP isolation. Silver staining revealed a discrete protein pattern in eluates of UV-irradiated samples that was consistent with similar experiments done in human and fruit fly cells (Fig 1G) [42,43]. This pattern was different from that of the whole cell lysate (inputs of the cRIC experiment), indicating that these isolated proteins were a subset of the cellular proteome. No proteins were detected in non-irradiated samples, further confirming that the isolated proteins were RBPs.

UUKV infection induces a reconfiguration of the tick RBPome

We next performed a quantitative proteomics analysis of the cRIC eluates. Quality control analyses revealed that (i) the overall protein intensity in UV cross-linked samples is far superior to that in non-irradiated counterparts (S2A Fig); and (ii) that the replicates clustered together in Principal Component Analysis (PCA) with UV irradiation explaining most of the variation (~85%), followed by whether cells were infected with UUKV (~6%) (S2B Fig). From these results it was established that data were of excellent quality and could be used for further analyses.

From the 572 identified proteins, 541 and 530 were enriched in UV-irradiated over non-irradiated samples at a false discovery rate (FDR) of 10% and 1%, respectively (Fig 2A and S1 Table). Due to the limited available information and annotation for ticks, we decided to include the full 10% FDR group for further analyses. To test if these proteins were RBPs, we first identified the human *(Homo sapiens*) and fruit fly *(Drosophila melanogaster*) orthologous proteins using InParanoid [37]; we found that 65% and 58% of the proteins within our dataset had human or fruit fly orthologs, respectively (Fig 2B). Approximately 80% of the 349 proteins with human orthologs have been experimentally determined to be RBPs (Fig 2C). Similarly, we observed that homologs of nearly 50% of the identified tick RBPome has previously been described as RNA binding in fly studies [43,44] (Fig 2D). Therefore, we concluded that the ISE6 tick RNA interactome is consistent with a *bona fide* RBPome.

Strikingly, 283 RBPs were differentially regulated in infected versus mock-infected cells at a 10% FDR (Fig 2E and S2 Table). Reassuringly, both the RNA-dependent RNA polymerase (L) and the viral nucleocapsid protein (N) were amongst the most enriched proteins in UUKV-infected cells compared to mock-infected samples, with N levels exhibiting the highest fold change observed. Gene set enrichment analysis revealed that RNAi silencing, processing of capped pre-mRNA, deadenylation and translation were the most upregulated pathways, while rRNA processing was depleted under infection conditions. Our results are consistent with the known importance of RNAi in the antiviral response of arthropods and translation in viral protein synthesis [45,46].

The UUKV N interactome and its connections with RBPome dynamics

Bunyaviral RNAs are found strongly associated with the viral nucleoprotein (N), which is one of the main components of the viral ribonucleoprotein (vRNP) complexes present in the cellular cytoplasm [47]. To survey the range of proteins associated with bunyaviral RNAs, we investigated the N protein interactome in UUKV-infected tick cells by using

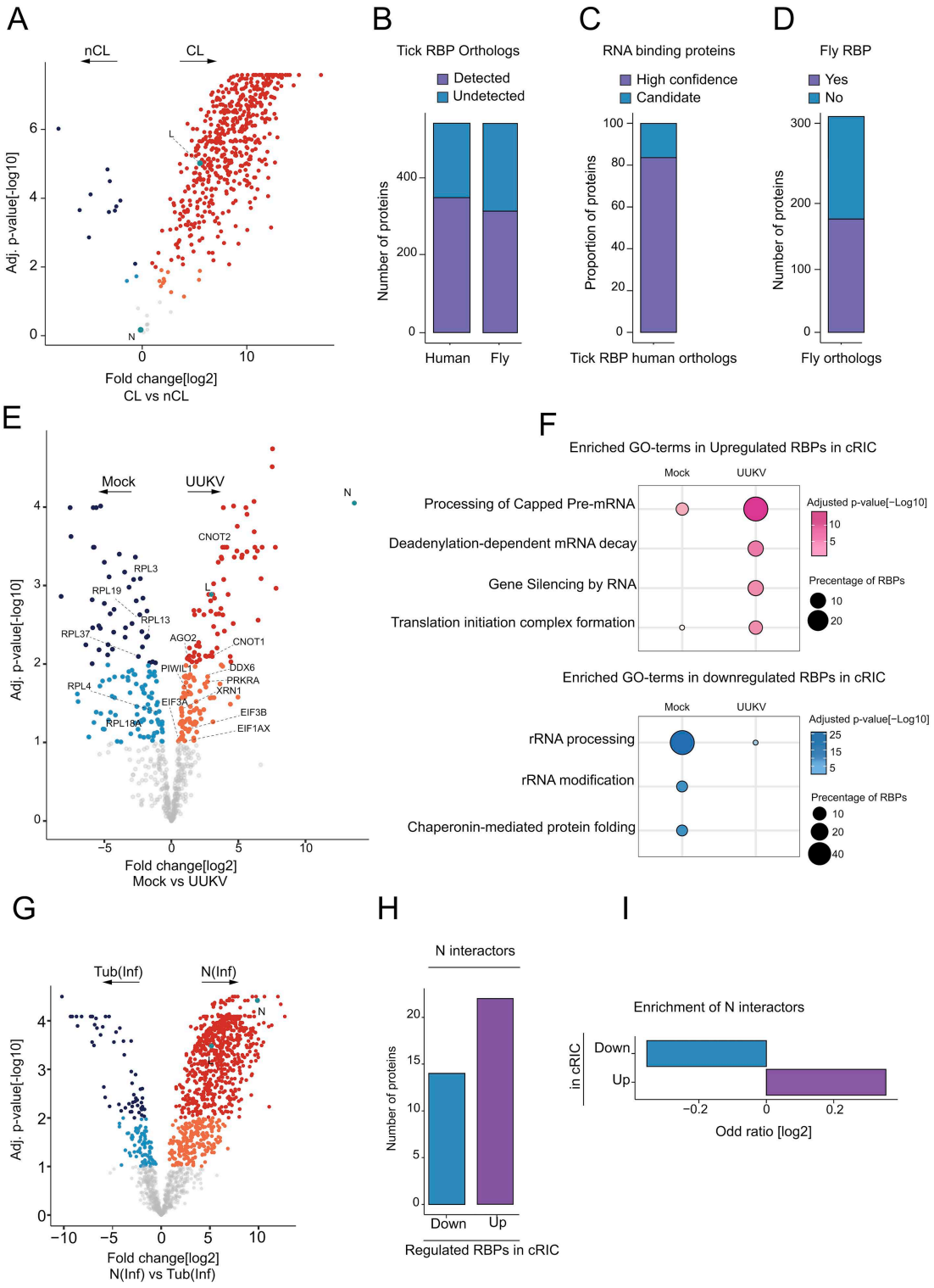

Fig 2. Differential regulation of the RBPome during UUKV- infection in ISE6 cells. (A) The fold changes in the proteins found in the UUKV-infected cross-linked (CL) samples compared to the non-cross-linked (nCL) samples (x-axis) were plotted against the significance of this fold change (Adj. p value[-log10], y axis). For proteins with a positive fold change, proteins at a 1-10% false discovery rate are coloured in orange and proteins at a 1% false discovery rate or below are coloured red. For proteins with a negative fold change, the false discovery rate groups are coloured light blue (1-10% FDR) and dark blue (1% FDR), respectively. (B) The numbers of proteins within the differential ISE6 RBPome with corresponding human and *Drosophila* (fly)

orthologs. (C) The human orthologs identified in (B) were compared against a defined experimentally proven database of RNA binding proteins (RBP-base v0.2.1 alpha). Proteins which were found by three independent comparisons were termed high confidence (purple), while the other proteins were termed candidates. (D) Percentage of IS6 RNA binding proteins with fly orthologs detected in previous RIC studies in flies. (E) The fold changes of the proteins identified in (A) were compared to the mock cross-linked samples (x axis; arrows indicate proteins enriched in either mock or UUKV-infected samples) and plotted against the significance of this fold change (Adj. p value[-log10], y axis). For proteins with a positive fold change, proteins at a 1-10% false discovery rate are coloured in orange and proteins at a 1% false discovery rate or below are coloured red. For proteins with a negative fold change, and therefore in higher quantities in non-cross-linked samples, proteins at a 1-10% FDR coloured in light blue, and proteins at a 1% FDR or below are coloured dark blue. Proteins with greater than 10% FDR are shown in grey. (F) Enrichment of cellular pathways in the upregulated (shown in pink) and downregulated (shown in blue) RNA binding proteins in the cRIC during UUKV- infection. (G) Comparison of fold changes of proteins found in the UUKV-infected samples using UUKV N [N (Inf)] or tubulin [Tub (inf)] antibody immunoprecipitation. (H) The number of differentially regulated RBPs in cRIC interacting with the viral nucleocapsid (N) protein. (I) The odds ratio of the N interactors found in the upregulated and downregulated RIC RBPs were calculated to determine the enrichment of the N interactors in the RIC data.

https://doi.org/10.1371/journal.ppat.1013393.g002

immunoprecipitation (IP) with highly specific antibodies. The proteomic data correlated well, and experimental triplicates clustered together in PCA analysis with 87.4% of the variance explained by infection status and 7.1% by the antibody used (i.e., against N or Tubulin) (S2 Fig). A total of 701 and 922 proteins were enriched in N over β-Tubulin IP conditions with 1% and 10% FDR, respectively (Fig 2G and S3 Table). In addition, 613 proteins were enriched in UUKV-infected cells over mock conditions at 10% FDR (S2D Fig and S3 Table). Both N protein and the RNA-dependent RNA polymerase (L) were enriched in infected conditions and over the β-Tubulin control IP. For a more stringent analysis, we cross-referenced the 10% FDR candidates described in the two different comparisons above (Figs 2G and S2D). A total of 378 proteins were consistently enriched in UUKV-infected vs mock and N vs β-Tubulin IP conditions (S2E Fig and S3 Table), and these were classified as N interactors.

We cross-referenced the N interactors with our previously generated differential RBPome (defined in Fig 2E). Of the 378 proteins immunoprecipitated from UUKV-infected cells, 14 and 22 proteins were found within the downregulated and upregulated RBP groups, respectively (Fig 2H and S3 Table). Interestingly, we found a modest enrichment of N interactors within the upregulated RIC data suggesting their direct involvement in vRNA metabolism (Fig 2I).

dsRNA knockdown of cellular RBPs regulates UUKV infection

To evaluate the roles of the UUKV-responsive RBPs and their importance in tick cell infection, we knocked down several candidates using dsRNA transfection (Fig 3). We utilised a previously optimised Magnetofection technology to deliver dsRNA into tick cells [48]. After dsRNA transfection, various parameters such as cell metabolic activity, UUKV N expression, intra- and extracellular viral RNA (RT-qPCR), and release of infectious virions (IFA analysis) were measured. Confocal microscopy analysis of UUKV-infected ISE6 monolayers showed a robust UUKV infection over the time course in both the mock- and dseGFP transfected monolayers. In contrast, transfection of a dsRNA targeting UUKV N almost completely abrogated UUKV infection (Fig 3A). No difference in UUKV RNA abundance, UUKV M copy number, or viral titre was observed in dseGFP-transfected monolayers compared to the mock-transfected samples. A modest but significant reduction in cell viability and N protein abundance was observed at days 6 and 9 p.i. in non-transfected rUUKV-infected samples relative to mock-infected controls, but this effect was not present in dseGFP-transfected cells. Notably, dseGFP transfection slightly increased viral titre at 9 days p.i. (Fig 3B), indicating that transfection alone can subtly modulate infection dynamics. However, transfection with UUKV N-targeting dsRNA caused a marked reduction in all infection parameters studied (Fig 3C), demonstrating that the identity of the dsRNA has a substantially greater effect than the process of transfection and validating the specificity and efficacy of our knockdown approach in tick cell cultures.

To assess the impact of the UUKV-responsive RBPs, we used the optimised protocol with dsRNAs against the mRNAs encoding our candidate RBPs or eGFP as control. Candidate RBPs were selected for dsRNA knockdown based on their presence in the 1% FDR cRIC dataset and prior implication of their orthologs in viral infection. While not all were dual interactors of viral RNA and N protein (as shown in Fig 3D), several did overlap with N interactors identified in our

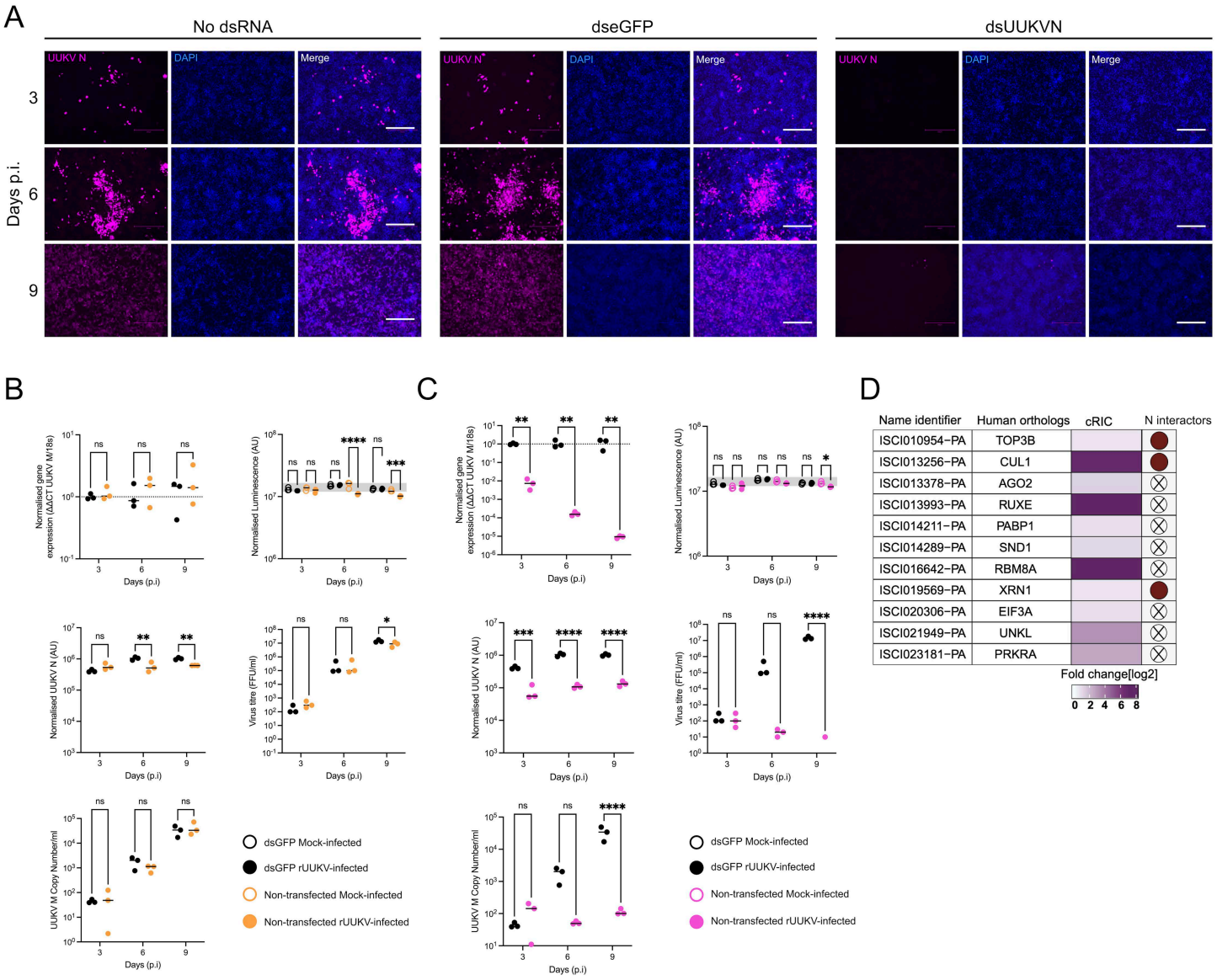

Fig 3. Effect of eGFP dsRNA or UUKV N dsRNA transfection on UUKV replication in infected ISE6 cells. (A) UUKV-infected, dsRNA-transfected cell monolayers, imaged at the time points indicated were stained using DAPI (blue) and mouse anti-UUKV N (purple). Imaging was carried out using an EVOS microscope, scale bar 300 μm. In parallel, cell monolayers were either transfected as (B) mock (black) vs dseGFP (orange) or (C) mock (black) vs dsUUKV N (pink) and were further analysed for additional parameters. These include quantity of intracellular UUKV M RNA (normalised ΔΔCT), cell metabolic activity (normalised luminescence), UUKV N expression via in well western blot (normalised UUKV N), UUKV titre (FFU/ml) and UUKV M RNA (UUKV M RNA copy number/ml) present in cell culture supernatant. Each gene type knockdown biological replicate was carried out conjointly with all other gene type knockdowns alongside the positive and negative controls. (D) Targets selected for knockdown analysis and their corresponding human orthologs. The fold change within the cRIC data [log2] is indicated in purple as defined in Fig 2D, alongside whether the protein is defined as an N interactor as specified in Fig 2G. Statistical significance was measured by ordinary two-way ANOVA with Sidak's multiple comparisons test. Asterisks indicates significance **** = $p < 0.0001$, *** = $p \leq 0.001$, ** = $p \leq 0.01$, * = $p \leq 0.05$, ns = not significant.

https://doi.org/10.1371/journal.ppat.1013393.g003

study. Most of the targeted transcripts were effectively depleted in transfected cells apart from *CUL1*, *PRKRA*, and *XRN1* genes that showed only 50% knockdown efficiency at late timepoints (S3 Fig). Commercially available antibodies against tick proteins are currently lacking and, therefore, RNA analysis by RT-qPCR is the only reliable method to assess gene

silencing. We also examined cell metabolic activity and found no effect over the eGFP control for most of the dsRNAs over the time course. However, a modest reduction in metabolic activity was observed in UUKV-infected samples at several timepoints for knockdowns targeting PABP1, and in a lesser extent for PRKRA and UNKL (S4 Fig). The potential effects of altered viral fitness will be discussed below.

Many of the RBP knockdowns resulted in a statistically significant increase in UUKV M segment RNA at either the 3- or 6-day time point (Fig 4). This is not unexpected considering the known antiviral roles of proteins such as the endonuclease AGO2 and the downstream exonuclease XRN1 in the arthropod RNAi system [21,49–51]. The knockdown of other genes involved in the translation of cellular mRNAs such as EIF3A and PABP1 also resulted in an increased accumulation of UUKV RNA in the cell. Conversely, TOP3B knockdown had no impact on UUKV M RNA levels (Fig 4).

To assess the virion assembly and release efficiency, both infective virus particles (Fig 5) and viral RNA (Fig 6) were quantified in the supernatant of infected cells. Only a small amount of infectious virus was detectable in the supernatant at 3 days p.i. (~ 10^2 FFU/ml) in the dseGFP treated control. This increased over time to ~10^6 FFU/ml by 9 days p.i. Surprisingly, the increased detection of UUKV M RNA in the knockdown cells observed in Fig 4 did not translate into an increase of infectious viral particles at the time points tested. An observable and significant decrease in the production of infectious UUKV was observed at 9 days p.i. in all knockdown samples except for UNKL and XRN1, in which no significant difference was observed (Fig 5).

Extracellular viral RNA is a proxy for the total number of released viral particles, including defective non-infectious particles. Both UNKL and XRN1 knockdown caused a decrease in the amount of viral RNA present in the supernatant with no overall effect on viral titre, suggesting that the knockdown of these genes may increase the infective to non-infective particle ratio (Figs 4 and 5). Conversely, TOP3B knockdown caused a decrease in viral titre with no effect on overall extracellular viral RNA levels, which indicates a reduction in viral particle infectivity. Altogether, our data revealed three RBPs (UNKL, XRN1 and TOP3B) with opposite effects on viral particle infectivity.

The AlphaFold structures for the *I. scapularis* ISCI010954 protein (i.e., TOP3B) and its *H. sapiens* ortholog show similar spatial arrangement of the topoisomerase-primase (TOPRIM) and DNA topoisomerase type IA domains (Fig 7A, upper panel), which are essential for TOP3B activity. Moreover, a study employing RBDmap revealed the peptide in the human TOP3B that crosslinks to RNA upon UV irradiation, which represents the RNA-binding surface of the protein. We determined *in silico* if this peptide is conserved in *I. scapularis* and found a striking sequence homology (Fig 7A, lower panel). This suggests that the human and tick TOP3B interact with RNA through the same protein-RNA interface. Interestingly the RNA-bound peptide sequence has higher sequence conservation (around 80%) than the rest of tryptic peptides across the protein sequence (around 60%), suggesting a selective pressure to maintain this sequence unaltered to keep TOP3B function (Fig 7B).

Discussion

Research into arboviruses that are transmitted by ticks have largely focussed on the interactions the virus establishes with vertebrate cells and systems. A major contributing factor to the dearth of research into tick-virus interactions has been the lack of characterised cell cultures with corresponding molecular tools, and the difficulties surrounding *in vivo* systems, as previously mentioned. The evolution of high-throughput technology and continuous characterisation of both cell cultures and whole organisms [52] has allowed the genomes of both the *I. scapularis* tick [53] and derived ISE6 cell line [17] to be annotated. From this, researchers have begun to probe into how tickborne arboviruses manipulate the vector cell to facilitate their own replication and transmission. Therefore, the focus of this study was to provide a comprehensive survey of the alterations in the RBPome triggered by an infecting virus in tick cells.

The advances in tick reagents and resources enabled us to apply comparative RIC to tick cells. The RBPome and its responses have been profiled in several species to date using RIC methodology, including humans [42], mice [54], fish (*Danio rerio*) [55], *Drosophila* spp. [43], parasites (*Leishmania* spp.) [56], yeast (*Saccharomyces cerevisiae*) [57], and

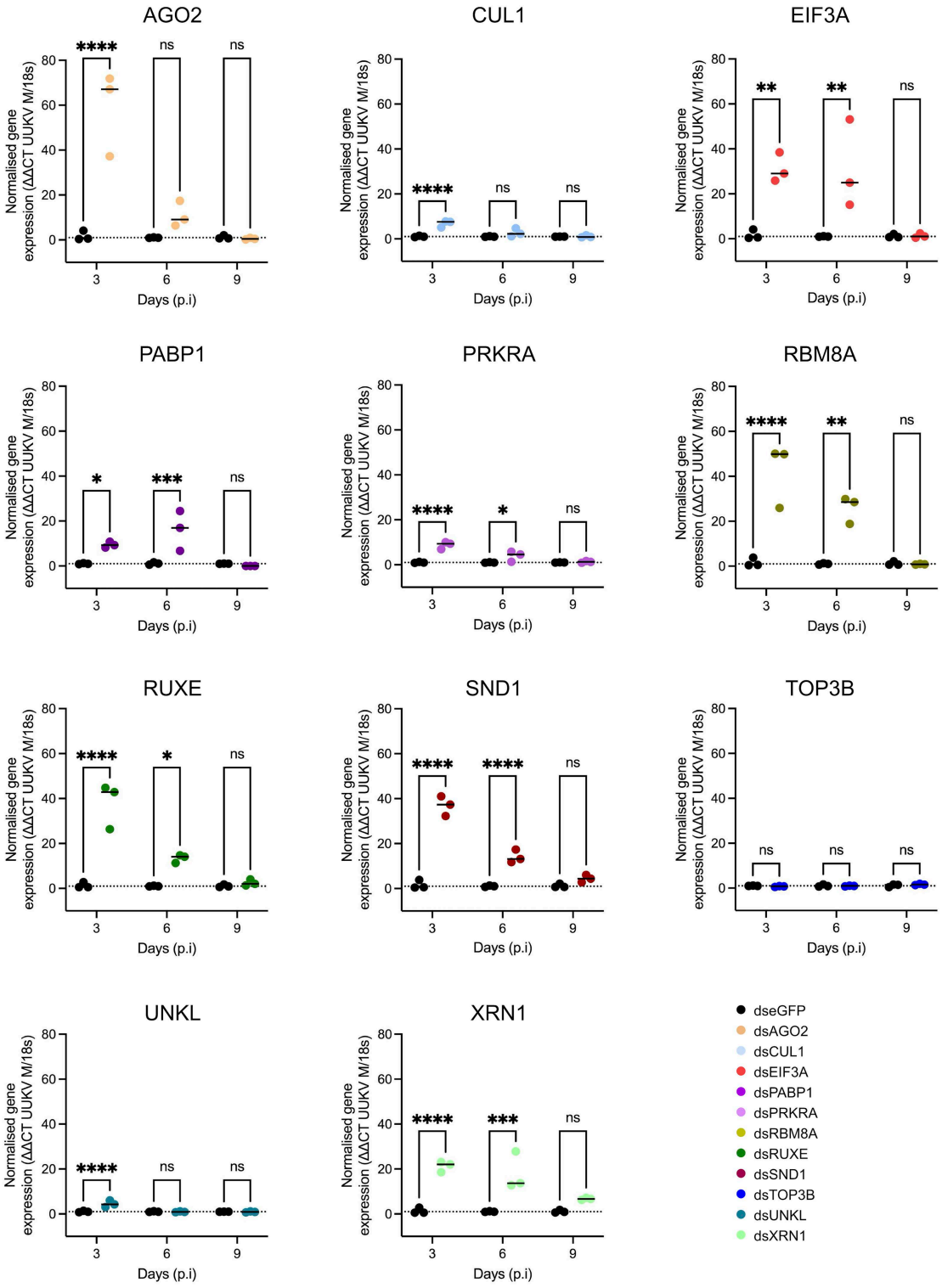

Fig 4. Effect of dsRNA transfections on the expression of UUKV M segment RNA levels within UUKV infected ISE6 cell culture. ISE6 cell monolayers were transfected with 2μg of dsRNA homologous to the indicated gene, before being infected with UUKV at an MOI of 5 in triplicate and harvested at the indicated timepoints. Data presented show the normalised expression of UUKV M RNA in UUKV-infected, dsRNA-transfected ISE6 cell monolayers, calculated using the ΔΔCt method. Black symbols represent dseGFP data (mock) and coloured symbols represent dsGene data. Statistical significance was measured by ordinary two-way ANOVA with Sidak's multiple comparisons test. Asterisks indicates significance ****=p<0.0001, ***=p≤0.001, **=p≤0.01, *=p≤0.05, ns=not significant.

https://doi.org/10.1371/journal.ppat.1013393.g004

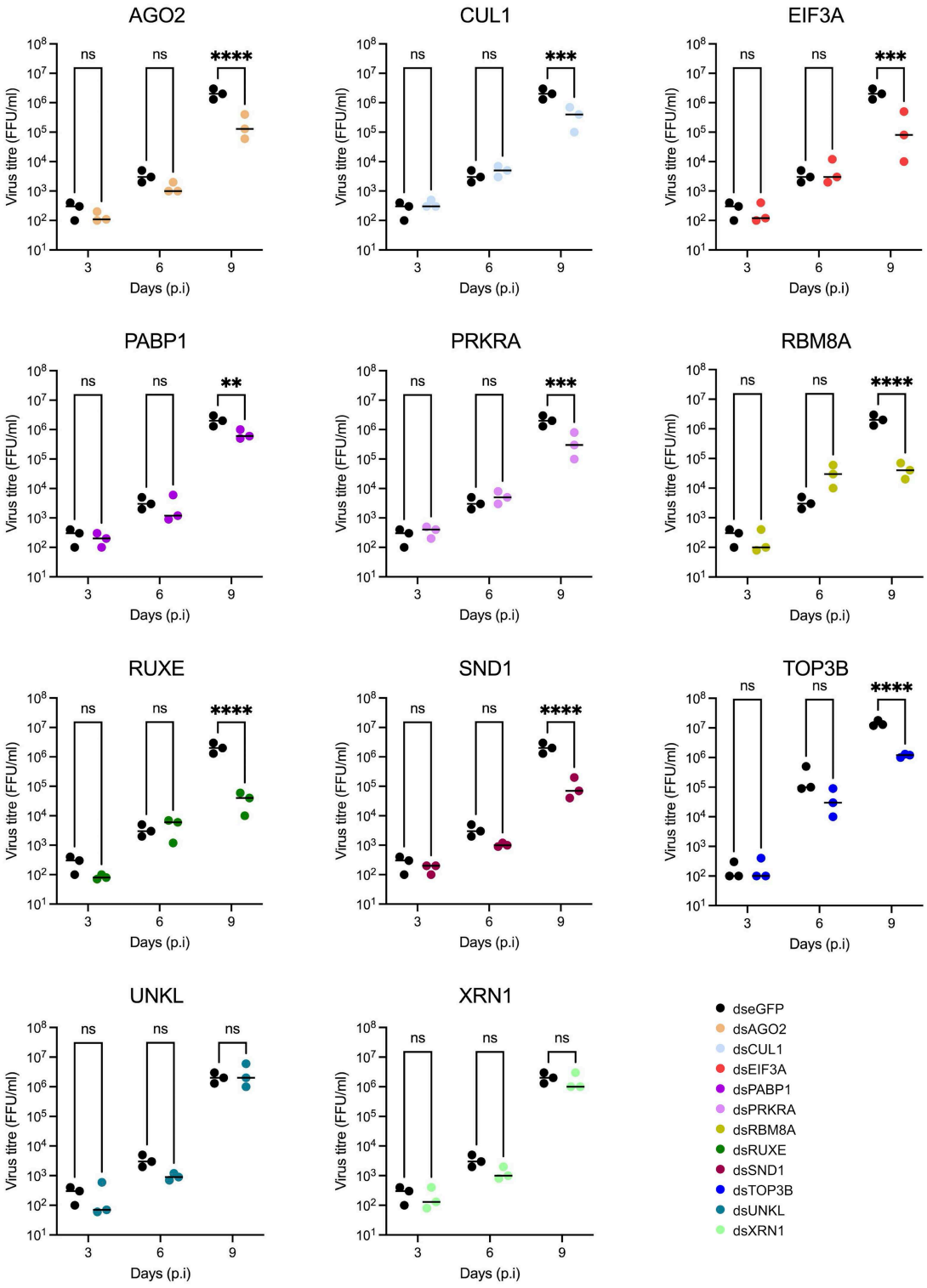

Fig 5. Effect of dsRNA transfections on UUKV titre in supernatant from UUKV-infected ISE6 cell cultures. UUKV titre of supernatant of UUKV-infected, dsRNA-transfected ISE6 cell monolayers, prepared as shown in Fig 4. Black symbols represent dseGFP data (mock) and coloured symbols represent dsGene data. Statistical significance was measured by ordinary two-way ANOVA with Sidak's multiple comparisons test. Asterisks indicates significance **** = $p < 0.0001$, *** = $p \leq 0.001$, ** = $p \leq 0.01$, * = $p \leq 0.05$, ns = not significant.

https://doi.org/10.1371/journal.ppat.1013393.g005

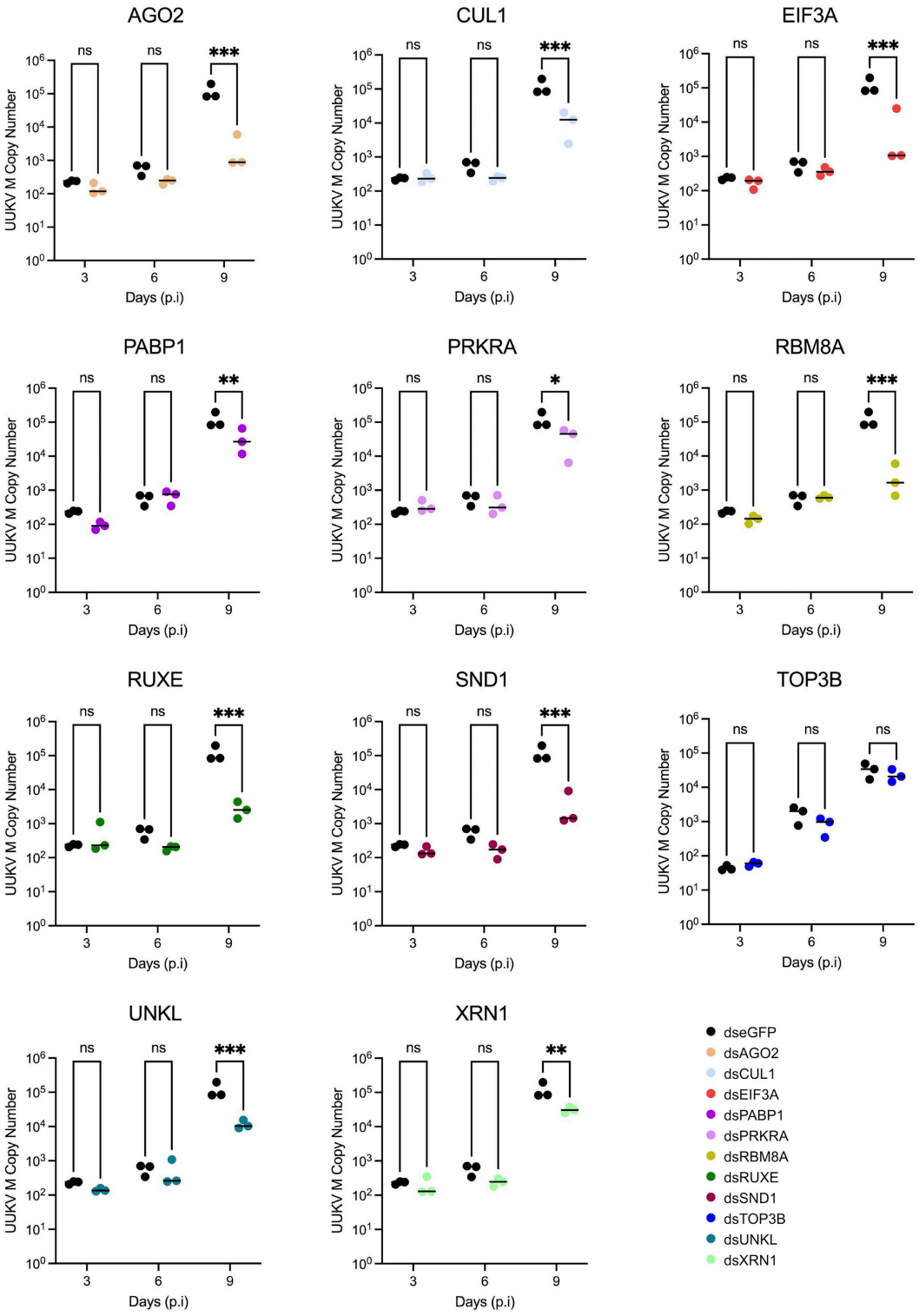

Fig 6. Effect of dsRNA transfections on quantity of UUKV M segment RNA present in supernatant of UUKV-infected ISE6 cell cultures. The copy number of UUKV M RNA within the supernatant of UUKV-infected, dsRNA-transfected ISE6 cell monolayers was determined as prepared as seen in Fig 4. Black symbols represent dseGFP data (mock) and coloured symbols represent dsGene data. Statistical significance was measured by ordinary two-way ANOVA with Sidak's multiple comparisons test. Asterisks indicates significance **** = $p < 0.0001$, *** = $p \leq 0.001$, ** = $p \leq 0.01$, * = $p \leq 0.05$, ns = not significant.

https://doi.org/10.1371/journal.ppat.1013393.g006

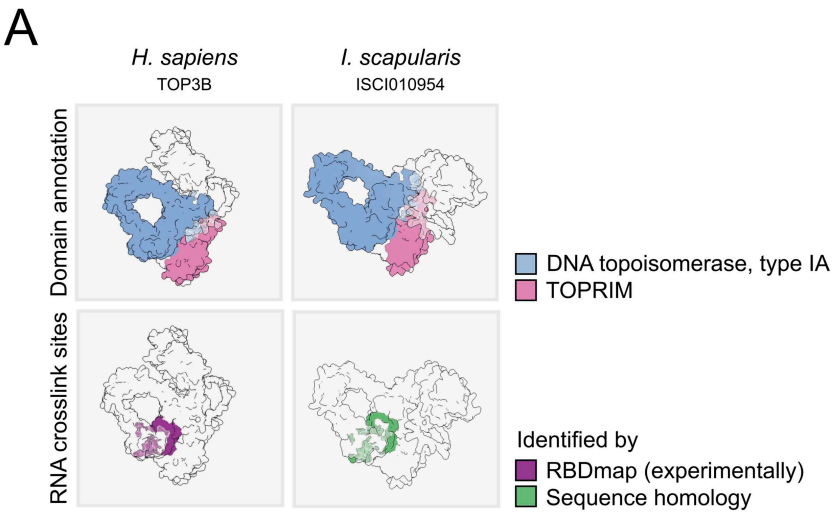

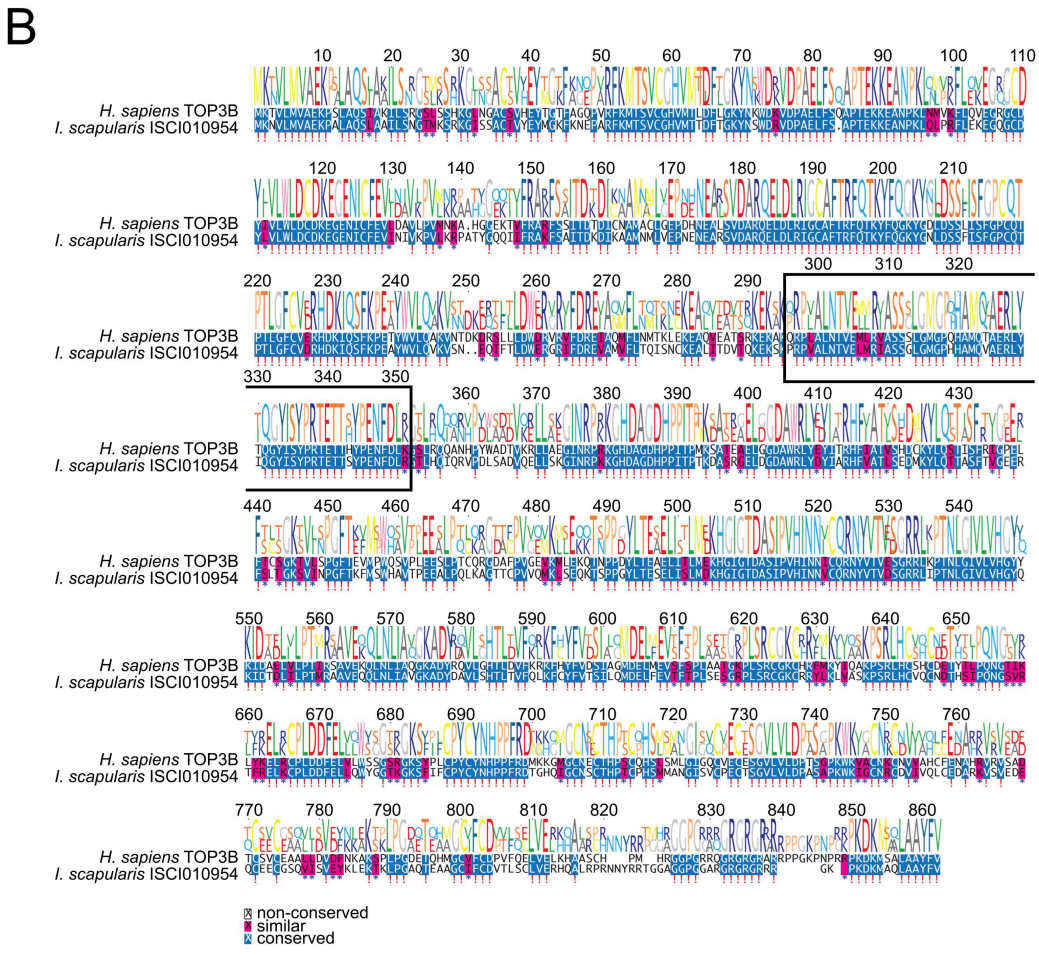

Fig 7. Structure and sequence similarities between *H. sapiens* TOP3B and *I. scapularis* ISCI010954 proteins. (A) AlphaFold structure for *H. sapiens* TOP3B and *I. scapularis* ISCI010954, highlighting the predicted domain annotations (in the upper panel) and the RNA crosslink sites (in the lower panel). (B) Protein sequences alignment of *H. sapiens* TOP3B and *I. scapularis* ISCI010954.

https://doi.org/10.1371/journal.ppat.1013393.g007

plants (*Arabidopsis thaliana*) [58]. In this manuscript we adapted the use of RIC to UUKV-infected ISE6 cell cultures and established a baseline methodology for investigating the effect of virus replication upon the infected tick cell. Despite bunyavirus mRNA molecules lacking a poly-A tail [40,41], the genome of UUKV contained sufficient poly-A like sequences to allow for viral RNA capture.

Therefore, both viral and cellular mRNA were isolated with the oligo(dT) pull down, contributing collectively to the composition of the RBPome. Strikingly, infection of tick cells with UUKV altered the RNA-binding profile of hundreds of RBPs in analogy to what occurs in humans [31,32]. These changes affected different pathways of RNA metabolism and are in line with a tick cell rewiring by two opposite processes: i) the virus activating or inactivating pathways that are required or detrimental (respectively) to infection; and ii) the host cell responding to this cue by triggering the antiviral program illustrated by AGO2, CNOT1 and XRN1. Moreover, a substantial proportion of regulated RBPs interacted with UUKV N in cells, suggesting a direct connection with viral ribonucleoproteins taking over the host RBP machinery and inducing changes to the intracellular RBPome. Several of the RBPs identified as impacting UUKV have pivotal roles in central machineries of RNA metabolism in both vertebrate and invertebrate cells. The phenotypes observed during the loss-of-function experiments could be due to a direct effect on viral RNA, as seen in other studies [59,60], or an indirect effect resulting from the disruption of a central pathway important for cell homeostasis. For example, depletion of the eukaryotic translation initiation factor 3a (eIF3a) and polyadenylate-binding protein 1 (PABP1) were found to increase the amount of UUKV M RNA in the cell at 3 and 6 days p.i. There are two possible mechanisms that could result in this observed increase in UUKV M RNA, either through eIF3a or PABP1 interacting with either viral or cellular RNA. It is unlikely that the activity of PABP1 is on stability or translation of UUKV RNAs because they lack poly(A) tails [40]. However, given our identification of 'poly(A)–like' regions within the UUKV genome, it is plausible that PABP1 exerts its effects through direct interaction with the viral RNA, although not mediated by an interaction with the viral nucleocapsid protein (Fig 3D). Recent work by Shalamova et al. [61] demonstrated that the Rift Valley fever virus (RVFV) genome is not fully coated with N protein, leaving RNase-sensitive regions of all three RNA segments exposed. Similar structural features may exist in the UUKV RNP, potentially permitting access by host RNA-binding proteins such as PABP1 [40].Therefore, we hypothesise that the PABP and eIF3a upregulation of viral gene expression is likely due to an indirect effect by suppressing the translation of cellular mRNAs by hijacking these factors [62] and increasing the availability of ribosomes for viral mRNAs. Other bunyaviruses such as RVFV utilise viral proteins (NSs) to target PABP1 for relocalisation in RVFV-infected human cell lines, creating an environment that favours viral translation suggesting a similar mechanism for UUKV in tick cells [63]. In addition, PABP1 is a key component of the closed-loop model of translation initiation, where it facilitates ribosome recruitment via interactions with eIF4G and eIF4E, and thus its depletion could broadly alter translation efficiency [64]. While the PABP1 effect aligns with the lack of poly(A) tail in UUKV RNAs, the sensitivity of UUKV gene expression to eIF3a knockdown suggests a partial but non-canonical reliance on eIF3. However, this effect does not imply full dependence and may reflect an alternative mechanism independent of both PABP and core eIF3 function, akin to IRES-like or other alternative mechanisms [65]. Other viruses encoding internal ribosome entry sites (IRES), such as hepatitis C virus (HCV) [66] and cricket paralysis virus (CrPV) [67] have been shown to have no or partial dependency on eIF3. However, no IRES has been reported at the 5' leader sequences of UUKV mRNAs, which are derived from the cap-snatching of the cellular mRNAs [68–70]. How these viral mRNAs translate independently of eIF3a and PABP is unknown and potential explanations such as the existence of a virus-encoded translation factor or the efficient liberation of ribosomes by the virus-induced shutoff should be explored in future. The increase in the level of UUKV RNA following dsRNA knockdown of eIF3a or PABP1, surprisingly, did not lead to an increase in the titre of released virus over the 9-day period. However, this may simply reflect the slow replication kinetics of UUKV within tick cells [2].

Other RBPs tested here are also components of central machineries involved in RNA metabolism, including RBM8A (exon junction complex) [71], RUXE (spliceosome) [72], SND1 (miRNA decay) [73] and XRN1 (mRNA decay) [51]. We observed phenotypes in UUKV infection for all these proteins, but whether they function indirectly through regulation of

cellular RNA metabolism or directly through binding to viral RNA, should be elucidated in future work. SND1, for example, could regulate UUKV expression through its influence on the set of RNAs available in the cell. However, recent work has shown that SND1 is critical to recruit NSP9 to the end of SARS-CoV2 RNA to initiate replication [74,75]. Hence, RBPs must be evaluated mechanistically on an individual basis and the indirect versus direct effects should be considered.

Changes in cell metabolism may reflect the importance of specific genes for cellular function (e.g., CUL1) or may result from enhanced virus replication triggering cytopathic effects (e.g., EIF3A, PRKRA). As noted, dsRNA transfection modestly reduces metabolism and N protein abundance during infection; however, when dsRNA targeted towards a gene is performed, we see a combined and specific effect from that transfection. Interestingly, UNKL and XRN1 knockdown reduced the amount of viral RNA detected in the cell culture supernatant without affecting overall viral titre, suggesting a compensatory mechanism such that the infectious:non-infectious particle ratio is increased in knockdown cells. This is a very curious finding that will warrant further mechanistic investigation. One of the most interesting results was that found with the knockdown of *ISCI010954* (ortholog of *TOP3B* in mammalian systems). TOP3B is a topoisomerase that changes the topological state of genetic material through breaking and then reforming genomic nucleic acid strands to unwind supercoils, resolve catenates, and undo knots [76]. This genetic material is usually double-stranded (ds)DNA. However, TOP3B is the only known topoisomerase to interact with both DNA and RNA [77]. TOP3B is dispersed within the cytoplasm and can interact with single stranded nucleic acids through an RGG box [77]. It is also speculated that TOP3B interacts with other RNA-binding proteins to regulate mRNA translation and may also increase the stability of mRNAs [78]. To further support our hypothesis that the ISCI010954 protein has a propensity to bind nucleic acids, we compared the predicted structure of this protein to the mammalian ortholog, TOP3B (Fig 7). To accomplish this, we utilised predicted AlphaFold structures of the human and tick proteins [79]. The *I. scapularis* ISCI010954 (i.e., TOP3B) protein and its *H. sapiens* ortholog show similar spatial arrangement of the topoisomerase-primase (TOPRIM) and DNA topoisomerase type IA domains (Fig 7A, upper panel), which are essential for TOP3B activity. Moreover, a study employing RBDmap revealed the peptide in the human TOP3B that crosslinks to RNA upon UV irradiation, which represents the RNA-binding surface of the protein. Using *in silico* methods, we determined if this peptide is conserved in *I. scapularis* and found a striking sequence homology (Fig 7A, lower panel) [80]. This suggests that the human and the tick TOP3B proteins interact with RNA through the same protein-RNA interface. Interestingly, the RNA-bound peptide sequence has higher sequence conservation (around 80%) than the rest of the tryptic peptides across the protein sequence (around 60%), suggesting a selective pressure to maintain this sequence unaltered to retain TOP3B function (Fig 7B).

TOP3B was reported to regulate the replication of several flaviviruses, but interestingly it was reported to not affect the replication of two negative sense viruses in mammalian systems [81]. In fact, several TOP proteins have been associated with viral RNA in mammalian systems, reviewed in Castello et al, 2024; highlighting the need for further experimentation to uncover the role of TOP proteins in infection from vectors to mammals [74]. Our results reveal that TOP3B knockdown does not affect UUKV replication but does impair the production of infectious viral particles, although the overall release of virions is unaffected. These striking results agree with previous work in mammalian cells infected with flaviviruses extending the reach of this phenomenon to different viral families and host species [81]. The impairment of infectious virus production following TOP3B depletion may reflect a role for topoisomerases in maintaining UUKV RNA in a functional conformation required for recognition by the N or L proteins and packaging into virions. As viral RNA levels in the supernatant remained unaffected, this effect is more likely due to the disruption of the functional conformation of the viral ribonucleoprotein complexes rather than reduced RNA stability. It is unclear if TOP3B itself is packaged into viral particles, however if this is the case it may be used to unwrap the UUKV RNA from the viral nucleocapsid to promote initial viral infection. While most topoisomerases bind DNA and have a nuclear subcellular localisation, under certain conditions, TOP3B can bind mRNAs associated with neuronal cell development in stress granules within the cytoplasmic compartment, and it is also necessary for normal synapse formation in both *D. melanogaster* and mice [82]. Given the predominantly neuronal-like phenotype of the ISE6 cell line [83,84], and the similarities between viral replication factories and stress

granules [85] within the cytoplasm of infected cells, it is tempting to speculate that TOP3B is performing a similar function in the infected tick cell and hence impacting virus replication.

Here we focused on the RBPs that were upregulated by UUKV infection; however, downregulated proteins might also be important in virus infection [31,32]. Our identification of several critical anti-viral RBPs within UUKV infection, which provides the foundation for not only analysis of conserved function across arbovirus species but also further investigation into the mechanisms of inhibition which may provide future therapeutic targets.

Materials and methods

Experimental model and subject detail

Cell culture. Mammalian cell cultures used in this study were BSR and BSR-T7/5-CL21 (referred to as BSR-T7) cells, provided by Karl-Klaus Conzelmann of Ludwig-Maximilians-Universität München. The BSR cell line is a clone of BHK-21 [86]. BSR-T7 cell cultures are a modified BSR cell line stably transfected with the bacteriophage T7 RNA polymerase [87]. Both cell lines were maintained in DMEM (Thermo Fisher Scientific) supplemented with 10% (v/v) foetal bovine serum (FBS) at 37°C in an atmosphere of 5% CO_2 in air. BSR-T7 cell medium was supplemented with 1mg/ml of the selection agent Geneticin (G418) prior to transfection. The tick cell line used in this study was ISE6, derived from embryonic *I. scapularis* [35], sourced from the Tick Cell Biobank at the University of Liverpool. The cells were grown in sealed, flat-sided tubes (Nunc) for maintenance and transferred to sealed T25 or T80 non-vented flasks to bulk them up for experiments. ISE6 cells were maintained at 32°C in enriched L-15B300 medium [88], supplemented with 10% tryptose phosphate broth, 5% FBS, 2 mM l-glutamine and 0.1% bovine lipoprotein concentrate (MP Biomedicals, Thermo-Fisher).

Virus production. UUKV used in this project was a recombinant UUKV generated using reverse genetic technologies and based upon the prototype tick isolate S-23 [3]. Working stocks of UUKV were generated from recombinant virus rescued in BSR-T7 cells, followed by amplification and generation of working stocks in BSR cell cultures. UUKV stocks were titrated using an immunofocus assay as described below.

Immunofocus assay. Virus titres were enumerated by an immunofocus assay in BSR cells. Briefly, confluent monolayers of BSR cells were infected with serial dilutions of virus made in phosphate buffer saline (PBS) containing 2% FBS and incubated for 1h at 37 °C, followed by the addition of a GMEM overlay supplemented with 2% FCS and 0.6% Avicel (FMC Biopolymer). The cells were incubated for 5 days before fixation and subsequent use in focus-forming assays as described previously [3,14].

RNA interactome capture (RIC)

Comparative RNA interactome capture (RIC) was performed following a previously described protocol [34], with the following modifications. ISE6 cells were seeded in six sets of 3 x 10 cm plates with 1.5 x 10^7 cells/plate. Cells were either mock-infected or inoculated with UUKV at a multiplicity of infection (MOI) of 5 FFU/cell. Samples were harvested from three replicate plates at 9 days p.i., when cells were washed 3x with PBS, then irradiated with 150 mJ/cm^2 of UV light at 254nm on ice and lysed with 3ml of lysis buffer (20mM Tris-HCl [pH 7.5], 500mM LiCl, 0.5% [w/v] LiDS, 1mM EDTA, 0.1% [v/v] IGPAL, and 5mM DTT) Lysates were then mechanically homogenised on ice by passing the sample through a 32G diameter needle using a 5ml syringe. A sample of homogenized lysate was removed at this stage for silver staining and qPCR analysis. Oligo$(dT)_{25}$ capture beads were equilibrated in lysis buffer, and 300µl of the vortexed bead slurry mix was added to each of the 6 samples and incubated for 1 h at 4°C with gentle rocking. Beads were collected in 1.5ml microcentrifuge tubes via a magnet, and the lysates removed and discarded. Beads were then washed as described below with lysis buffer, wash buffer 1 (20mM Tris-HCl [pH 7.5], 500mM LiCl, 1mM EDTA, 0.01% [v/v] IGEPAL, and 5mM DTT), wash buffer 2 (20mM Tris-HCl [pH 7.5], 500mM LiCl, 1mM EDTA, 0.01% [v/v] IGPAL, and 5mM DTT) on ice, followed by wash buffer 3 (Oligo(dT) buffer 3: 20mM Tris0HCl [pH 7.5], 200mM LiCl, 1mM EDTA, and 5mM DTT) at room temperature. To

wash, 1ml of the appropriate buffer was added to the beads. The beads were inverted 10 times per minute, for 5 min, whilst being stored on ice or at room temperature as specified. The beads were washed 3 times with each of the buffers utilised in the protocol. Beads were resuspended in 125µl of elution buffer (20mM Tris-HCl [pH 7.5] and 1mM EDTA) and incubated for 3 min at 55°C with agitation. Finally, prepared eluates were stored at -80°C.

Coimmunoprecipitation

Coimmunoprecipitation (co-IP) was carried out using ISE6 cell monolayers infected with UUKV at a MOI of 5 FFU/cell, as described above. Mouse anti-UUKV N antibodies, generated from hybridoma 8B11A3 (kindly provided by Dr Anna Överby Wernstedt, Umeå University [89]) were cross-linked to Dynabeads Protein G (Thermo Fisher) using BS3 (bis(sulfosuccinimidyl)suberate) following the manufacturer's instructions. Antibody cross-linked beads were prepared for use in immunoprecipitation by washing in 500µl of lysis buffer (20mM Tris, 150mM NaCl, 5mM MgCl2, 0.5% [v/v] NP40, 25 unit/ml Benzonase (Merck Millipore), fresh cOmplete protease inhibitor [1 tablet per 10ml of buffer], phosphatase inhibitor [Roche, 1 tablet per 10ml of buffer] per 100µl bead mix with gentle rotation at 4°C for five min and finally stored in lysis buffer at 4°C.At 9 days p.i., cells were lysed in 1ml of lysis buffer per plate. Cell lysates from either mock or UUKV-infected triplicate plates were pooled and kept on ice.

Supernatants were clarified by centrifugation for 20 min at 5000 rpm and 4°C and transferred to fresh 15 ml centrifuge tubes where 100µl of the lysates were removed for analysis by silver staining.

Prepared antibody-cross-linked beads were incubated with the cleared lysates and incubated with gentle rotation at 4°C overnight. Beads were then collected using a magnet, and the supernatant discarded. Beads were washed with 500µl of wash buffer (50mM Tris, 200mM NaCl, 1mM EDTA, 1% [v/v] NP40, fresh cOmplete protease inhibitor [1 tablet per 10ml/ buffer]) with gentle rotation at 4°C for five min. Washing was repeated three times then the proteins were eluted by incubation of the beads with 125µl of elution buffer (100mM TEAB, 5% SDS [w/v]) at 95°C for 10 min. Protein eluates were stored at -80°C prior to subsequent analysis.

Synthesis of double-stranded RNA (dsRNA)

RNA was extracted from ISE6 cells using TRIzol (Invitrogen), following the chloroform extraction protocol. Reverse transcription (RT) was carried out using the SuperScript Reverse Transcriptase kit (Invitrogen) and random hexamers (50µM) to produce cDNAs corresponding to cellular or viral targets (listed in S4 Table). Unique portions of the gene candidates were amplified from the prepared cDNAs with primers incorporating a minimal T7 RNA polymerase promoter sequence (All primer sequences can be found in S4 Table). PCR products were analysed by agarose gel electrophoresis and purified by gel extraction. PCR products were sequenced for target verification before the production of dsRNA. The MEGAscript RNAi Kit (Thermo Fisher Scientific) was used to produce the dsRNA from the PCR fragments, according to the manufacturer's instructions. To determine the quality of the dsRNA, the concentration was determined using a Nanodrop One. Once prepared dsRNAs were stored at -80°C.

dsRNA knockdown in tick cells

ISE6 cells were seeded into 24-well plates and monolayers were transfected using the Magnetofectamine O2 transfection kit (1ug of dsRNA/1x10^6 cells), at the indicated ratio of dsRNA:transfection reagent, 2µl of magnetofectamine beads, and 250µl OptiMEM (Gibco), following the manufacturer's protocol (Oz Biosciences). After transfection, the transfection medium was removed, and fresh medium applied. Monolayers were then incubated for 20 h before infection with UUKV at a MOI of 5 FFU/cell. Cell monolayers were harvested at the time points indicated and analysed using RT qPCR, cell metabolic activity assays, whole cell immunofluorescence analysis, and focus-forming assay to assess the production of infectious virus particles.

Whole cell immunofluorescence analysis

For immunofluorescence analysis of UUKV-infected cultures, culture supernatants were removed, and monolayers washed with PBS. Cells were fixed in 8% formaldehyde solution for 1 h and permeabilised in permeabilization buffer (0.5% [v/v] Triton X-100 [Roth] in PBS) for 30 min. For both primary and secondary antibody buffers, the corresponding antibodies (Mouse anti-UUKV generated from hybridoma 8B11A3 and Anti-mouse IgG (H&L) Secondary Invitrogen #T6199, respectively) were diluted in blocking buffer (4% (w/v) skimmed milk powder (Marvel) in PBST - 0.1% (v/v) Tween [Sigma] in PBS). The cell monolayers were then washed three times with PBS before being probed with primary antibody buffer. Primary antibody incubation was carried out overnight at 4°C. Cells were then washed three times with PBS before being probed for 1 h at room temperature with secondary antibody. Cells were washed once with PBS before being incubated with DAPI diluted in PBS (3µl:10mL buffer) for 10 min at room temperature. Finally, cell monolayers were washed three times with PBS. Cells were kept at 4°C in PBS until imaging. Monolayers were imaged using an Odyssey CLx Imaging System (Li-Cor) and analysed using the associated software to determine the total UUKV N fluorescence compared to a mock-infected well as a control.

Cell metabolic activity assay

CellTiter-Glo 2.0 Cell Viability Assay (Promega) was used to determine the metabolic activity of transfected cell monolayers. At the appropriate timepoint, cell monolayers were washed before being resuspended in 150µl of fresh PBS. 50µl of the cell suspension or PBS control was pipetted into opaque-walled 94 well plates in triplicates. The cell suspension was then mixed with 50µl of viability reagent and incubated in the dark for 10 min at room temperature. Well luminescence was measured using the GloMax Navigator Microplate Luminometer (Promega).

Reverse-transcription and quantitative PCR

RNA was isolated from cell monolayers or infected cell supernatant using TRIzol, following the chloroform extraction protocol (Invitrogen). Reverse transcription (RT) to generate cDNA was carried out using the SuperScript Reverse Transcriptase kit and random hexamers (50µM; Thermo Fisher Scientific), following the manufacturer's instructions. Positive controls were generated from randomly primed cDNA derived from either total cell RNA or UUKV-infected cell culture supernatant. For negative controls, cDNA was replaced with nuclease-free H2O. qPCR primers for UUKV were designed to target the genomic M segment RNA. qPCR analysis was undertaken using SYBR-green (Applied Biosystems) on a QuantStudio 5 Real-Time PCR System (Applied Biosystems) and associated software. Details of the primers used for qPCR in this study can be found in S5 Table. Transcript expression levels relative to the ISE6 18S ribosomal subunit as a reference were calculated according to the $2^{-\Delta\Delta CT}$ methodology [90]. Where no housekeeping gene was present to allow for the ΔΔCt calculation, such as when isolating UUKV M RNA from supernatant, Ct values were normalized, or a standard curve was produced to allow gene copy number to be determined. The maximum detection limit for the thermocycler was defined as a Ct of 40, and negative controls produced a Ct of 30 or above. Therefore, any samples which produced a normalised Ct ≤ 10 were therefore classified as a negative result.

Conventional protein analysis

If cell monolayers were not lysed through prior protocols, lysis of mock or UUKV-infected cell monolayers was carried out using Laemmli buffer (100mM Tris-HCl, 4% (v/v) SDS, 20% (v/v) glycerol, 200mM DTT, 0.2% bromophenol blue (v/v), 3µl/ml endonuclease). Samples were resolved on SDS-PAGE and visualised via Pierce Silver Stain Kit (Thermo Fisher Scientific #24612) and/or by western blotting using mouse anti-UUKV N and anti-mouse IgG (H&L) secondary, the Li-Cor Odyssey system for visualization and the Image Studio Lite software (Li-Cor) for quantification. Data shown in the manuscript are representative gels from at least three independent replicates.

Mass spectrometry and relative protein quantification

RIC and viral nucleocapsid protein (N) pulldown eluates were processed through single-pot solid-phase-enhanced (SP3) as previously described [42] and SDS-PAGE followed by in-gel digestion (with trypsin treatment) sample preparation, respectively.

After SP3 processing, prepared samples of ISE6 RIC were analysed at the Rosalind Franklin Institute. Analysis of peptides was carried out using an Ultimate 3000 nano-LC 1000 system coupled to an Orbitrap Fusion Lumos (Thermo Fisher Scientific). Samples were diluted in ultra-pure water with 5% formic acid and 5% DMSO prior to injection. Peptides were initially trapped on a C18 PepMap100 pre-column (300 µm inner diameter x 5 mm, 100A) and then separated on an in-house built C18 column (Reprosil-Gold, Dr. Maisch, 1.9 µm particle size) column (ID: 50 µm, length: 50 cm) at a flow rate of 100 nL/min. Peptides were separated over 60 min using mobile phase A (water and 5% DMSO, 0.1% formic acid) and a 12–30% gradient of mobile phase B (acetonitrile and 5% DMSO, 0.1% formic acid). Separated peptides were directly electro-sprayed into an Orbitrap Fusion Lumos mass spectrometer (Thermo Fisher Scientific) and analysed in a data-dependent mode. MS1 spectra were acquired in the orbitrap (350–1400 m/z, resolution 60000, AGC target 1.2 x 10^6, maximum injection time 50 ms). The top 40 most abundant peaks in the survey scan were fragmented using HCD and analysed in the ion trap (scan speed Turbo, AGC target 1 x10^4, maximum injection time 32 ms, normalised collision energy 30%).

Nucleocapsid protein pulldown eluates were sent to the Dundee FingerPrints Proteomics facility for mass-spectrometry analysis (in data-dependent mode and label-free quantification). Samples were resolved via 1D SDS-PAGE on a 10% gel with MOPS buffer and stained with Quick Coomassie Stain (Generon). Each gel lane was run for 15 min with the whole area being excised, then subjected to in-gel digestion using 1mg/ml Trypsin (Thermo) at a final concentration of 12.5µg/mL. Digested peptides were run on a Q-Exactive HF (Thermo Scientific) instrument coupled to a Dionex Ultimate 3000 HPLC system (Thermo Scientific). A 2–35%B gradient comprising of eluent A (0.1% formic acid) and eluent B (80% acetonitrile/0.1% formic acid) was used to run a 120-minute gradient per sample. The top 20 most intense peaks from a mass range of 335–1800 m/z in each MS1 scan with a resolution of 60,000 were then taken for MS2 analysis at a resolution of 15,000. Spectra were fragmented using Higher-energy C-trap dissociation (HCD).

The raw data files were provided upon completion for all eluate samples. Protein identification and quantification were obtained using the Andromeda search engine implemented in MaxQuant (v.2.0.3.0) and searched against the ISE6 reference proteome (downloaded on 16/12/2022) [19] and UUKV proteome (AAA47958.1, AAA47959.1, AAA79512.1 & BAA01590.1; downloaded from NCBI 06/05/2015) [28] with 'match between run' activated and under default parameters.

MaxQuant outputs (proteinGroups) were used for downstream relative quantification. Potential protein contaminants flagged by MaxQuant were filtered out together with proteins with missing values across all samples, using R-package "DEP (1.4.1)",. For relative quantification between UV-crosslinked versus non-crosslinked infected samples, protein raw intensities were $\log_2$-transformed. Missing value imputation was performed only for proteins undetected in all replicates in one experimental condition, while present in the other condition (in at least 2 replicates). Imputation was implemented using minimum determination method (Mindet) [64]. Next, the processed protein intensities were subjected to statistical analysis using the empirical Bayesian method moderated t-test with p-values adjusted for multiple-testing (Benjamini-Hochberg method) provided by R-package "limma (3.38.3)" for. For all other comparisons, protein intensities were processed as described above with inclusion of a normalization step for raw protein intensities using R-package Variance Stabilizing Normalization "VSN (3.50.0)".

Protein ortholog identification

To identify human (Uniprot_id: UP000005640, downloaded Nov2016) and fly (Uniprot_id: UP000000803, downloaded Aug2024) orthologs of ISE6 proteins InParanoid-DIAMOND was used under default settings [37,91].

Reactome enrichment analysis

Enrichment analysis of cellular pathways in differentially regulated RNA binding proteins was performed by R package ReactomePA. The analysis only included ISE6 proteins with human orthologs and all human genes as background [92].

Structure prediction, protein domains and RNA crosslink sites annotation

Using ColabFold [93] in batch mode we predicted protein structures. We exported the "relaxed_rank_001_alphafold2" pdb file to Chimerax v1.7 for visualization [94]. Protein domains identified by InterProScan [95] and RNA crosslink sites identified by RBDmap [80] or by sequence homology by ClustalOmega [96].

Quantification and statistical analysis

For each condition, biological triplicates were produced, where each biological sample was tested (for example by RT qPCR) in triplicate, and an average of the technical replicates was then used for plotting and statistical analysis. Testing for statistical significance was carried out by either unpaired t-test, one-way ANOVA, or two-way ANOVA with Sidak's multiple comparison. The cut-off for significance was set at $p < 0.05$. Where analysis was employed, unless stated otherwise both "ns" and a lack of notation indicate no significance.

Supporting information

S1 Fig. Additional qPCR data detecting UUKV S and L RNA in RIC samples, supporting Fig 1F. (A) Quantity of UUKV S RNA within input and eluate samples of ISE6 cell monolayers treated by RIC. (B) Quantity of UUKV LRNA within input and eluate samples of ISE6 cell monolayers treated by RIC.
(TIFF)

S2 Fig. Diagnostics of mass spectrometry results from RIC biological triplicates and immunoprecipitation biological triplicates, and further analysis of immunoprecipitation mass spectrometry results. Diagnostics of mass spectrometry data derived from rUUKV-infected cRIC eluates as described in Fig 1 and mock or rUUKV-infected immunoprecipitation eluates as described in Fig 2. (A) The protein intensities (intensity[log2], y axis) for all proteins found within each triplicate sample (x axis) of each condition; mock or rUUKV infected, crosslinked or non-crosslinked, were plotted from rUUKV-infected cRIC eluates. (B) Principal component analysis (PCA) was performed from rUUKV-infected cRIC eluates. The plot models 91.5% of the total data variance. Variance proportions are shown along both axes, and groupings of the triplicates for each sample are highlighted on the plot. (C) Principal component analysis (PCA) was performed for mass spectrometry results of mock or rUUKV-infected immunoprecipitation eluates. The plot models 94.1% of the total data variance. Variance proportions are shown along both axes, and groupings of the triplicates for each sample are highlighted on the plot. (D) The fold change in the proteins specific to UUKV N immunoprecipitation in mock- and rUUKV-infected cells (x axis) were plotted against the significance of this fold change (Adj. p value[-log10], y axis). Proteins with a positive fold change, 1–10% FDR (orange), ≤ 1% (red); proteins with a negative fold change, 1–10% FDR (light blue), ≤ 1% (dark blue) and proteins with greater than 10% FDR are shown in grey. (E) The infected cell tubulin vs UUKV N protein pulldown (Fig 2F) and mock infected vs UUKV infected UUKV N pulldown (S1D Fig) was cross-referenced to identify proteins within both groups, of which 378 proteins were found to be present in both groups.
(TIFF)

S3 Fig. Effect of dsRNA transfections on selected gene expression within ISE6 cell culture. Triplicate ISE6 cell monolayers were transfected with 2μg of dsRNA homologous to the indicated gene. Black symbols represent dseGFP data (mock) and coloured symbols represent dsGene data. At one day post-transfection, cell monolayers were infected with rUUKV at 5 FFU/cell. At timepoints indicated, cell monolayers were lysed via TRIzol and cellular RNA extracted. RT

qPCR was performed on the cellular RNA using primers against the indicated gene, and I. scapularis ribosomal 18S as the 'housekeeping' gene. The normalised expression of UUKV M RNA was calculated using the 2-ΔΔCt method. Statistical significance was measured by ordinary two-way ANOVA with Sidak's multiple comparisons test. Asterisks indicate significance **** = $p < 0.0001$, *** = $p \leq 0.001$, ** = $p \leq 0.01$, * = $p \leq 0.05$, ns = not significant.
(TIFF)

S4 Fig. Effect of dsRNA transfections on the metabolic activity within UUKV infected ISE6 cell culture. Triplicate ISE6 cell monolayers were transfected with 2μg of dsRNA homologous to the indicated gene. Black symbols represent dseGFP data (mock) and coloured symbols represent dsGene data. Shaded grey area indicates the variability of viability observed between mock infected samples. At one day post-transfection, cell monolayers were mock-infected (open circles) or infected with rUUKV at 5 FFU/cell (closed circles). At timepoints indicated, cell monolayers were washed with PBS before cell viability was analysed using CellTitre-Glo 2.0 Cell Viability Assay kit (Promega). Luminescence was measured using a GloMax plate reader. Sample luminescence was normalised against blank wells containing only media. Statistical significance was measured by ordinary two-way ANOVA with Sidak's multiple comparisons test. Asterisks indicate significance **** = $p < 0.0001$, *** = $p \leq 0.001$, ** = $p \leq 0.01$, * = $p \leq 0.05$, ns = not significant.
(TIFF)

S1 Table. UUKV-infected ISE6 RBPome. Comparison between UV-irradiated and non-irradiated UUKV-infected samples.
(XLSX)

S2 Table. Differentially regulated RBPs during UUKV infection. Comparison between UUKV-infected and mock-infected UV-irradiated samples.
(XLSX)

S3 Table. UUKV N interactome. (A) Comparison between immunoprecipitation of N and β-Tubulin from UUKV-infected samples. (B) Comparison between immunoprecipitation of N from UUKV-infected and mock-infected samples. (C) A total of 378 proteins were consistently enriched in UUKV-infected vs mock and N vs β-Tubulin IP conditions. (D) cross-reference of N interactors with differential regulated RBPome during UUKV infection.
(XLSX)

S4 Table. Table of oligonucleotide primers used in the production of double stranded RNA, including primer name, sequence and description of use.
(DOCX)

S5 Table. Table of oligonucleotide primers used in qPCR analysis, including primer name, sequence and description of use.
(DOCX)

Acknowledgments

We thank Prof. Ulrike Munderloh, University of Minnesota, for permission to use the ISE6 cell line.

Author contributions

Conceptualization: Wael Kamel, Alain Kohl, Alfredo Castello, Benjamin Brennan.

Data curation: Alexandra Wilson, Wael Kamel, Douglas Lamont, Yana Demyanenko, Alfredo Castello, Benjamin Brennan.

Formal analysis: Alexandra Wilson, Wael Kamel, Zaydah R De Laurent, Rozeena Arif, Andrew T Clarke, Douglas Lamont, Yana Demyanenko, Marko Noerenberg, Shabaz Mohammed, Alfredo Castello, Benjamin Brennan.

Funding acquisition: Shabaz Mohammed, Alfredo Castello, Benjamin Brennan.

Investigation: Alexandra Wilson, Wael Kamel, Kelsey Davies, Andrew T Clarke, Yana Demyanenko, Marko Noerenberg.

Methodology: Alexandra Wilson, Wael Kamel, Zaydah R De Laurent, Rozeena Arif, Douglas Lamont, Shabaz Mohammed, Alfredo Castello, Benjamin Brennan.

Project administration: Alfredo Castello, Benjamin Brennan.

Resources: Alexandra Wilson, Wael Kamel, Kelsey Davies, Andrew T Clarke, Lesley Bell-Sakyi, Marko Noerenberg, Shabaz Mohammed, Alfredo Castello, Benjamin Brennan.

Supervision: Alain Kohl, Shabaz Mohammed, Alfredo Castello, Benjamin Brennan.

Validation: Alexandra Wilson, Wael Kamel, Alfredo Castello, Benjamin Brennan.

Visualization: Alexandra Wilson, Wael Kamel, Zaydah R De Laurent, Rozeena Arif, Alfredo Castello, Benjamin Brennan.

Writing – original draft: Alexandra Wilson, Wael Kamel, Alfredo Castello, Benjamin Brennan.

Writing – review & editing: Alexandra Wilson, Wael Kamel, Kelsey Davies, Andrew T Clarke, Lesley Bell-Sakyi, Douglas Lamont, Yana Demyanenko, Marko Noerenberg, Alain Kohl, Shabaz Mohammed, Alfredo Castello, Benjamin Brennan.

References

1. Oker-Blom N, Salminen A, Brummer-Korvenkontio M, Kaeaeriaeinen L, Weckstroem P. Isolation of some viruses other than typical tick-borne encephalitis viruses from ixodes ricinus ticks In Finland. Ann Med Exp Biol Fenn. 1964;42:109–12. PMID: 14229542
2. Mazelier M, Rouxel RN, Zumstein M, Mancini R, Bell-Sakyi L, Lozach P-Y. Uukuniemi Virus as a Tick-Borne Virus Model. J Virol. 2016;90(15):6784–98. https://doi.org/10.1128/JVI.00095-16 PMID: 27194760
3. Rezelj VV, Överby AK, Elliott RM. Generation of mutant Uukuniemi viruses lacking the nonstructural protein NSs by reverse genetics indicates that NSs is a weak interferon antagonist. J Virol. 2015;89(9):4849–56. https://doi.org/10.1128/JVI.03511-14 PMID: 25673721
4. Pettersson RF, Hewlett MJ, Baltimore D, Coffin JM. The genome of Uukuniemi virus consists of three unique RNA segments. Cell. 1977;11(1):51–63. https://doi.org/10.1016/0092-8674(77)90316-6 PMID: 872219
5. Ranki M, Pettersson RF. Uukuniemi virus contains an RNA polymerase. J Virol. 1975;16(6):1420–5. https://doi.org/10.1128/JVI.16.6.1420-1425.1975 PMID: 517
6. Overby AK, Pettersson RF, Grünewald K, Huiskonen JT. Insights into bunyavirus architecture from electron cryotomography of Uukuniemi virus. Proc Natl Acad Sci U S A. 2008;105(7):2375–9. https://doi.org/10.1073/pnas.0708738105 PMID: 18272496
7. Lozach P-Y, Kühbacher A, Meier R, Mancini R, Bitto D, Bouloy M, et al. DC-SIGN as a receptor for phleboviruses. Cell Host Microbe. 2011;10(1):75–88. https://doi.org/10.1016/j.chom.2011.06.007 PMID: 21767814
8. Lozach P-Y, Mancini R, Bitto D, Meier R, Oestereich L, Overby AK, et al. Entry of bunyaviruses into mammalian cells. Cell Host Microbe. 2010;7(6):488–99. https://doi.org/10.1016/j.chom.2010.05.007 PMID: 20542252
9. Meier R, Franceschini A, Horvath P, Tetard M, Mancini R, von Mering C, et al. Genome-wide small interfering RNA screens reveal VAMP3 as a novel host factor required for Uukuniemi virus late penetration. J Virol. 2014;88(15):8565–78. https://doi.org/10.1128/JVI.00388-14 PMID: 24850728
10. Elliott RM, Brennan B. Emerging phleboviruses. Curr Opin Virol. 2014;5(100):50–7. https://doi.org/10.1016/j.coviro.2014.01.011 PMID: 24607799
11. Malet H, Williams HM, Cusack S, Rosenthal M. The mechanism of genome replication and transcription in bunyaviruses. PLoS Pathog. 2023;19(1):e1011060. https://doi.org/10.1371/journal.ppat.1011060 PMID: 36634042
12. Eifan SA, Elliott RM. Mutational analysis of the Bunyamwera orthobunyavirus nucleocapsid protein gene. J Virol. 2009;83(21):11307–17. https://doi.org/10.1128/JVI.01460-09 PMID: 19710139
13. Mottram TJ, Li P, Dietrich I, Shi X, Brennan B, Varjak M, et al. Mutational analysis of Rift Valley fever phlebovirus nucleocapsid protein indicates novel conserved, functional amino acids. PLoS Negl Trop Dis. 2017;11(12):e0006155. https://doi.org/10.1371/journal.pntd.0006155 PMID: 29267287
14. Rezelj VV, Li P, Chaudhary V, Elliott RM, Jin D-Y, Brennan B. Differential Antagonism of Human Innate Immune Responses by Tick-Borne Phlebovirus Nonstructural Proteins. mSphere. 2017;2(3):e00234-17. https://doi.org/10.1128/mSphere.00234-17 PMID: 28680969

15. Palacios G, Savji N, Travassos da Rosa A, Guzman H, Yu X, Desai A, et al. Characterization of the Uukuniemi virus group (Phlebovirus: Bunyaviridae): evidence for seven distinct species. J Virol. 2013;87(6):3187–95. https://doi.org/10.1128/JVI.02719-12 PMID: 23283959
16. Salata C, Moutailler S, Attoui H, Zweygarth E, Decker L, Bell-Sakyi L. How relevant are in vitro culture models for study of tick-pathogen interactions? Pathog Glob Health. 2021;115(7–8):437–55. https://doi.org/10.1080/20477724.2021.1944539 PMID: 34190676
17. Miller JR, Koren S, Dilley KA, Harkins DM, Stockwell TB, Shabman RS, et al. A draft genome sequence for the Ixodes scapularis cell line, ISE6. F1000Res. 2018;7:297. https://doi.org/10.12688/f1000research.13635.1 PMID: 29707202
18. Jia N, Wang J, Shi W, Du L, Sun Y, Zhan W, et al. Large-Scale Comparative Analyses of Tick Genomes Elucidate Their Genetic Diversity and Vector Capacities. Cell. 2020;182(5):1328-1340.e13. https://doi.org/10.1016/j.cell.2020.07.023 PMID: 32814014
19. Gulia-Nuss M, Nuss AB, Meyer JM, Sonenshine DE, Roe RM, Waterhouse RM, et al. Genomic insights into the Ixodes scapularis tick vector of Lyme disease. Nat Commun. 2016;7:10507. https://doi.org/10.1038/ncomms10507 PMID: 26856261
20. Bell-Sakyi L, Zweygarth E, Blouin EF, Gould EA, Jongejan F. Tick cell lines: tools for tick and tick-borne disease research. Trends Parasitol. 2007;23(9):450–7. https://doi.org/10.1016/j.pt.2007.07.009 PMID: 17662657
21. Schnettler E, Tykalová H, Watson M, Sharma M, Sterken MG, Obbard DJ, et al. Induction and suppression of tick cell antiviral RNAi responses by tick-borne flaviviruses. Nucleic Acids Res. 2014;42(14):9436–46. https://doi.org/10.1093/nar/gku657 PMID: 25053841
22. Weisheit S, Villar M, Tykalová H, Popara M, Loecherbach J, Watson M, et al. Ixodes scapularis and Ixodes ricinus tick cell lines respond to infection with tick-borne encephalitis virus: transcriptomic and proteomic analysis. Parasit Vectors. 2015;8:599. https://doi.org/10.1186/s13071-015-1210-x PMID: 26582129
23. Grabowski JM, Gulia-Nuss M, Kuhn RJ, Hill CA. RNAi reveals proteins for metabolism and protein processing associated with Langat virus infection in Ixodes scapularis (black-legged tick) ISE6 cells. Parasit Vectors. 2017;10(1):24. https://doi.org/10.1186/s13071-016-1944-0 PMID: 28086865
24. McNally KL, Mitzel DN, Anderson JM, Ribeiro JMC, Valenzuela JG, Myers TG, et al. Differential salivary gland transcript expression profile in Ixodes scapularis nymphs upon feeding or flavivirus infection. Ticks Tick Borne Dis. 2012;3(1):18–26. https://doi.org/10.1016/j.ttbdis.2011.09.003 PMID: 22309855
25. Mansfield KL, Cook C, Ellis RJ, Bell-Sakyi L, Johnson N, Alberdi P, et al. Tick-borne pathogens induce differential expression of genes promoting cell survival and host resistance in Ixodes ricinus cells. Parasit Vectors. 2017;10(1):81. https://doi.org/10.1186/s13071-017-2011-1 PMID: 28202075
26. Simser JA, Macaluso KR, Mulenga A, Azad AF. Immune-responsive lysozymes from hemocytes of the American dog tick, Dermacentor variabilis and an embryonic cell line of the Rocky Mountain wood tick, D. andersoni. Insect Biochem Mol Biol. 2004;34(12):1235–46. https://doi.org/10.1016/j.ibmb.2004.07.003 PMID: 15544937
27. Sidak-Loftis LC, Rosche KL, Pence N, Ujczo JK, Hurtado J, Fisk EA, et al. The Unfolded-Protein Response Triggers the Arthropod Immune Deficiency Pathway. mBio. 2022;13(4):e0070322. https://doi.org/10.1128/mbio.00703-22 PMID: 35862781
28. Uckeley ZM, Moeller R, Kühn LI, Nilsson E, Robens C, Lasswitz L, et al. Quantitative Proteomics of Uukuniemi Virus-host Cell Interactions Reveals GBF1 as Proviral Host Factor for Phleboviruses. Mol Cell Proteomics. 2019;18(12):2401–17. https://doi.org/10.1074/mcp.RA119.001631 PMID: 31570497
29. Castello A, Iselin L. Viral RNA Is a Hub for Critical Host-Virus Interactions. Subcell Biochem. 2023;106:365–85. https://doi.org/10.1007/978-3-031-40086-5_13 PMID: 38159234
30. Bermudez Y, Hatfield D, Muller M. A Balancing Act: The Viral-Host Battle over RNA Binding Proteins. Viruses. 2024;16(3):474. https://doi.org/10.3390/v16030474 PMID: 38543839
31. Garcia-Moreno M, Noerenberg M, Ni S, Järvelin AI, González-Almela E, Lenz CE, et al. System-wide Profiling of RNA-Binding Proteins Uncovers Key Regulators of Virus Infection. Mol Cell. 2019;74(1):196-211.e11. https://doi.org/10.1016/j.molcel.2019.01.017 PMID: 30799147
32. Kamel W, Noerenberg M, Cerikan B, Chen H, Järvelin AI, Kammoun M, et al. Global analysis of protein-RNA interactions in SARS-CoV-2-infected cells reveals key regulators of infection. Mol Cell. 2021;81(13):2851-2867.e7. https://doi.org/10.1016/j.molcel.2021.05.023 PMID: 34118193
33. Lisy S, Rothamel K, Ascano M. RNA Binding Proteins as Pioneer Determinants of Infection: Protective, Proviral, or Both? Viruses. 2021;13(11):2172. https://doi.org/10.3390/v13112172 PMID: 34834978
34. Castello A, Horos R, Strein C, Fischer B, Eichelbaum K, Steinmetz LM, et al. System-wide identification of RNA-binding proteins by interactome capture. Nat Protoc. 2013;8(3):491–500. https://doi.org/10.1038/nprot.2013.020 PMID: 23411631
35. Kurtti TJ, Munderloh UG, Andreadis TG, Magnarelli LA, Mather TN. Tick cell culture isolation of an intracellular prokaryote from the tick Ixodes scapularis. J Invertebr Pathol. 1996;67(3):318–21. https://doi.org/10.1006/jipa.1996.0050 PMID: 8812616
36. Iselin L, Palmalux N, Kamel W, Simmonds P, Mohammed S, Castello A. Uncovering viral RNA-host cell interactions on a proteome-wide scale. Trends Biochem Sci. 2022;47(1):23–38. https://doi.org/10.1016/j.tibs.2021.08.002 PMID: 34509361
37. Perez-Perri JI, Noerenberg M, Kamel W, Lenz CE, Mohammed S, Hentze MW, et al. Global analysis of RNA-binding protein dynamics by comparative and enhanced RNA interactome capture. Nat Protoc. 2021;16(1):27–60. https://doi.org/10.1038/s41596-020-00404-1 PMID: 33208978
38. Olschewski S, Cusack S, Rosenthal M. The Cap-Snatching Mechanism of Bunyaviruses. Trends Microbiol. 2020;28(4):293–303. https://doi.org/10.1016/j.tim.2019.12.006 PMID: 31948728

39. Ruscica V, Iselin L, Hull R, Embarc-Buh A, Narayanan S. XRN1 supplies free nucleotides to feed alphavirus replication. bioRxiv. 2024.
40. Blakqori G, van Knippenberg I, Elliott RM. Bunyamwera orthobunyavirus S-segment untranslated regions mediate poly(A) tail-independent translation. J Virol. 2009;83(8):3637–46. https://doi.org/10.1128/JVI.02201-08 PMID: 19193790
41. Bouloy M, Pardigon N, Vialat P, Gerbaud S, Girard M. Characterization of the 5' and 3' ends of viral messenger RNAs isolated from BHK21 cells infected with Germiston virus (Bunyavirus). Virology. 1990;175(1):50–8. https://doi.org/10.1016/0042-6822(90)90185-t PMID: 2309451
42. Castello A, Fischer B, Eichelbaum K, Horos R, Beckmann BM, Strein C, et al. Insights into RNA biology from an atlas of mammalian mRNA-binding proteins. Cell. 2012;149(6):1393–406. https://doi.org/10.1016/j.cell.2012.04.031 PMID: 22658674
43. Sysoev VO, Fischer B, Frese CK, Gupta I, Krijgsveld J, Hentze MW, et al. Global changes of the RNA-bound proteome during the maternal-to-zygotic transition in Drosophila. Nat Commun. 2016;7:12128. https://doi.org/10.1038/ncomms12128 PMID: 27378189
44. Wessels H-H, Imami K, Baltz AG, Kolinski M, Beldovskaya A, Selbach M, et al. The mRNA-bound proteome of the early fly embryo. Genome Res. 2016;26(7):1000–9. https://doi.org/10.1101/gr.200386.115 PMID: 27197210
45. Schuster S, Miesen P, van Rij RP. Antiviral RNAi in Insects and Mammals: Parallels and Differences. Viruses. 2019;11(5):448. https://doi.org/10.3390/v11050448 PMID: 31100912
46. Berkhout B, Haasnoot J. The interplay between virus infection and the cellular RNA interference machinery. FEBS Lett. 2006;580(12):2896–902. https://doi.org/10.1016/j.febslet.2006.02.070 PMID: 16563388
47. Hornak KE, Lanchy J-M, Lodmell JS. RNA Encapsidation and Packaging in the Phleboviruses. Viruses. 2016;8(7):194. https://doi.org/10.3390/v8070194 PMID: 27428993
48. Petit MJ, Flory C, Gu Q, Fares M, Lamont D, Score A, et al. Multi-omics analysis of SFTS virus infection in Rhipicephalus microplus cells reveals antiviral tick factors. Nat Commun. 2025;16(1):4732. https://doi.org/10.1038/s41467-025-59565-w PMID: 40399277
49. Scherer C, Knowles J, Sreenu VB, Fredericks AC, Fuss J, Maringer K, et al. An Aedes aegypti-Derived Ago2 Knockout Cell Line to Investigate Arbovirus Infections. Viruses. 2021;13(6):1066. https://doi.org/10.3390/v13061066 PMID: 34205194
50. Xu Y, Zhong Z, Ren Y, Ma L, Ye Z, Gao C, et al. Antiviral RNA interference in disease vector (Asian longhorned) ticks. PLoS Pathog. 2021;17(12):e1010119. https://doi.org/10.1371/journal.ppat.1010119 PMID: 34860862
51. Molleston JM, Cherry S. Attacked from All Sides: RNA Decay in Antiviral Defense. Viruses. 2017;9(1):2. https://doi.org/10.3390/v9010002 PMID: 28054965
52. Bell-Sakyi L, Hartley CS, Khoo JJ, Forth JH, Palomar AM, Makepeace BL. New Cell Lines Derived from European Tick Species. Microorganisms. 2022;10(6):1086. https://doi.org/10.3390/microorganisms10061086 PMID: 35744603
53. De S, Kingan SB, Kitsou C, Portik DM, Foor SD, Frederick JC, et al. A high-quality Ixodes scapularis genome advances tick science. Nat Genet. 2023;55(2):301–11. https://doi.org/10.1038/s41588-022-01275-w PMID: 36658436
54. Kwon SC, Yi H, Eichelbaum K, Föhr S, Fischer B, You KT, et al. The RNA-binding protein repertoire of embryonic stem cells. Nat Struct Mol Biol. 2013;20(9):1122–30. https://doi.org/10.1038/nsmb.2638 PMID: 23912277
55. Despic V, Dejung M, Gu M, Krishnan J, Zhang J, Herzel L, et al. Dynamic RNA-protein interactions underlie the zebrafish maternal-to-zygotic transition. Genome Res. 2017;27(7):1184–94. https://doi.org/10.1101/gr.215954.116 PMID: 28381614
56. Nandan D, Thomas SA, Nguyen A, Moon K-M, Foster LJ, Reiner NE. Comprehensive Identification of mRNA-Binding Proteins of Leishmania donovani by Interactome Capture. PLoS One. 2017;12(1):e0170068. https://doi.org/10.1371/journal.pone.0170068 PMID: 28135300
57. Tsvetanova NG, Klass DM, Salzman J, Brown PO. Proteome-wide search reveals unexpected RNA-binding proteins in Saccharomyces cerevisiae. PLoS One. 2010;5(9):e12671. https://doi.org/10.1371/journal.pone.0012671 PMID: 20844764
58. Marondedze C, Thomas L, Serrano NL, Lilley KS, Gehring C. The RNA-binding protein repertoire of Arabidopsis thaliana. Sci Rep. 2016;6:29766. https://doi.org/10.1038/srep29766 PMID: 27405932
59. Kang D, Gao S, Tian Z, Zhang G, Guan G, Liu G, et al. ISG20 inhibits bluetongue virus replication. Virol Sin. 2022;37(4):521–30. https://doi.org/10.1016/j.virs.2022.04.010 PMID: 35513266
60. Nencioni L, De Chiara G, Sgarbanti R, Amatore D, Aquilano K, Marcocci ME, et al. Bcl-2 expression and p38MAPK activity in cells infected with influenza A virus: impact on virally induced apoptosis and viral replication. J Biol Chem. 2009;284(23):16004–15. https://doi.org/10.1074/jbc.M900146200 PMID: 19336399
61. Shalamova L, Barth P, Pickin MJ, Kouti K, Ott B, Humpert K, et al. Nucleocapsids of the Rift Valley fever virus ambisense S segment contain an exposed RNA element in the center that overlaps with the intergenic region. Nat Commun. 2024;15(1):7602. https://doi.org/10.1038/s41467-024-52058-2 PMID: 39217162
62. Castelló A, Franco D, Moral-López P, Berlanga JJ, Alvarez E, Wimmer E, et al. HIV- 1 protease inhibits Cap- and poly(A)-dependent translation upon eIF4GI and PABP cleavage. PLoS One. 2009;4(11):e7997. https://doi.org/10.1371/journal.pone.0007997 PMID: 19956697
63. Copeland AM, Altamura LA, Van Deusen NM, Schmaljohn CS. Nuclear relocalization of polyadenylate binding protein during rift valley fever virus infection involves expression of the NSs gene. J Virol. 2013;87(21):11659–69. https://doi.org/10.1128/JVI.01434-13 PMID: 23966414
64. Sonenberg N, Hinnebusch AG. Regulation of translation initiation in eukaryotes: mechanisms and biological targets. Cell. 2009;136(4):731–45. https://doi.org/10.1016/j.cell.2009.01.042 PMID: 19239892

65. Valášek LS, Zeman J, Wagner S, Beznosková P, Pavlíková Z, Mohammad MP, et al. Embraced by eIF3: structural and functional insights into the roles of eIF3 across the translation cycle. Nucleic Acids Res. 2017;45(19):10948–68. https://doi.org/10.1093/nar/gkx805 PMID: 28981723

66. Sun C, Querol-Audí J, Mortimer SA, Arias-Palomo E, Doudna JA, Nogales E, et al. Two RNA-binding motifs in eIF3 direct HCV IRES-dependent translation. Nucleic Acids Res. 2013;41(15):7512–21. https://doi.org/10.1093/nar/gkt510 PMID: 23766293

67. Kerr CH, Ma ZW, Jang CJ, Thompson SR, Jan E. Molecular analysis of the factorless internal ribosome entry site in Cricket Paralysis virus infection. Sci Rep. 2016;6:37319. https://doi.org/10.1038/srep37319 PMID: 27853311

68. Hopkins K, Cherry S. Bunyaviral cap-snatching vs. decapping: recycling cell cycle mRNAs. Cell Cycle. 2013;12(24):3711–2. https://doi.org/10.4161/cc.26878 PMID: 24145225

69. Ho JSY, Angel M, Ma Y, Sloan E, Wang G, Martinez-Romero C, et al. Hybrid Gene Origination Creates Human-Virus Chimeric Proteins during Infection. Cell. 2020;181(7):1502-1517.e23. https://doi.org/10.1016/j.cell.2020.05.035 PMID: 32559462

70. Vera-Otarola J, Castillo-Vargas E, Angulo J, Barriga FM, Batlle E, Lopez-Lastra M. The viral nucleocapsid protein and the human RNA-binding protein Mex3A promote translation of the Andes orthohantavirus small mRNA. PLoS Pathog. 2021;17:e1009931 10.1371/journal.ppat.1009931

71. Salicioni AM, Xi M, Vanderveer LA, Balsara B, Testa JR, Dunbrack RL Jr, et al. Identification and structural analysis of human RBM8A and RBM8B: two highly conserved RNA-binding motif proteins that interact with OVCA1, a candidate tumor suppressor. Genomics. 2000;69(1):54–62. https://doi.org/10.1006/geno.2000.6315 PMID: 11013075

72. Fautsch MP, Wieben ED. Transcriptional regulation of the small nuclear ribonucleoprotein E protein gene. Identification of cis-acting sequences with homology to genes encoding ribosomal proteins. J Biol Chem. 1991;266(34):23288–95. PMID: 1835977

73. Tsuchiya N, Ochiai M, Nakashima K, Ubagai T, Sugimura T, Nakagama H. SND1, a component of RNA-induced silencing complex, is up-regulated in human colon cancers and implicated in early stage colon carcinogenesis. Cancer Res. 2007;67(19):9568–76. https://doi.org/10.1158/0008-5472.CAN-06-2707 PMID: 17909068

74. Castello A, Álvarez L, Kamel W, Iselin L, Hennig J. Exploring the expanding universe of host-virus interactions mediated by viral RNA. Mol Cell. 2024;84(19):3706–21. https://doi.org/10.1016/j.molcel.2024.08.027 PMID: 39366356

75. Schmidt N, Ganskih S, Wei Y, Gabel A, Zielinski S, Keshishian H, et al. SND1 binds SARS-CoV-2 negative-sense RNA and promotes viral RNA synthesis through NSP9. Cell. 2023;186(22):4834-4850.e23. https://doi.org/10.1016/j.cell.2023.09.002 PMID: 37794589

76. Pommier Y, Nussenzweig A, Takeda S, Austin C. Human topoisomerases and their roles in genome stability and organization. Nat Rev Mol Cell Biol. 2022;23(6):407–27. https://doi.org/10.1038/s41580-022-00452-3 PMID: 35228717

77. Ahmad M, Shen W, Li W, Xue Y, Zou S, Xu D, et al. Topoisomerase 3β is the major topoisomerase for mRNAs and linked to neurodevelopment and mental dysfunction. Nucleic Acids Res. 2017;45(5):2704–13. https://doi.org/10.1093/nar/gkw1293 PMID: 28039324

78. Siaw GE-L, Liu I-F, Lin P-Y, Been MD, Hsieh T-S. DNA and RNA topoisomerase activities of Top3β are promoted by mediator protein Tudor domain-containing protein 3. Proc Natl Acad Sci U S A. 2016;113(38):E5544-51. https://doi.org/10.1073/pnas.1605517113 PMID: 27582462

79. Jumper J, Evans R, Pritzel A, Green T, Figurnov M, Ronneberger O, et al. Highly accurate protein structure prediction with AlphaFold. Nature. 2021;596(7873):583–9. https://doi.org/10.1038/s41586-021-03819-2 PMID: 34265844

80. Castello A, Fischer B, Frese CK, Horos R, Alleaume A-M, Foehr S, et al. Comprehensive Identification of RNA-Binding Domains in Human Cells. Mol Cell. 2016;63(4):696–710. https://doi.org/10.1016/j.molcel.2016.06.029 PMID: 27453046

81. Diosa-Toro M, Prasanth KR, Bradrick SS, Garcia Blanco MA. Role of RNA-binding proteins during the late stages of Flavivirus replication cycle. Virol J. 2020;17(1):60. https://doi.org/10.1186/s12985-020-01329-7 PMID: 32334603

82. Xu D, Shen W, Guo R, Xue Y, Peng W, Sima J, et al. Top3β is an RNA topoisomerase that works with fragile X syndrome protein to promote synapse formation. Nat Neurosci. 2013;16(9):1238–47. https://doi.org/10.1038/nn.3479 PMID: 23912945

83. Oliver JD, Chávez ASO, Felsheim RF, Kurtti TJ, Munderloh UG. An Ixodes scapularis cell line with a predominantly neuron-like phenotype. Exp Appl Acarol. 2015;66(3):427–42. https://doi.org/10.1007/s10493-015-9908-1 PMID: 25894426

84. Mateos-Hernández L, Pipová N, Allain E, Henry C, Rouxel C, Lagrée A-C, et al. Enlisting the Ixodes scapularis Embryonic ISE6 Cell Line to Investigate the Neuronal Basis of Tick-Pathogen Interactions. Pathogens. 2021;10(1):70. https://doi.org/10.3390/pathogens10010070 PMID: 33466622

85. Brownsword MJ, Locker N. A little less aggregation a little more replication: Viral manipulation of stress granules. Wiley Interdiscip Rev RNA. 2023;14(1):e1741. https://doi.org/10.1002/wrna.1741 PMID: 35709333

86. Sato M, Maeda N, Yoshida H, Urade M, Saito S. Plaque formation of herpes virus hominis type 2 and rubella virus in variants isolated from the colonies of BHK21/WI-2 cells formed in soft agar. Arch Virol. 1977;53(3):269–73. https://doi.org/10.1007/BF01314672 PMID: 193466

87. Buchholz UJ, Finke S, Conzelmann KK. Generation of bovine respiratory syncytial virus (BRSV) from cDNA: BRSV NS2 is not essential for virus replication in tissue culture, and the human RSV leader region acts as a functional BRSV genome promoter. J Virol. 1999;73(1):251–9. https://doi.org/10.1128/JVI.73.1.251-259.1999 PMID: 9847328

88. Munderloh UG, Jauron SD, Fingerle V, Leitritz L, Hayes SF, Hautman JM, et al. Invasion and intracellular development of the human granulocytic ehrlichiosis agent in tick cell culture. J Clin Microbiol. 1999;37(8):2518–24. https://doi.org/10.1128/JCM.37.8.2518-2524.1999 PMID: 10405394

89. Persson R, Pettersson RF. Formation and intracellular transport of a heterodimeric viral spike protein complex. J Cell Biol. 1991;112(2):257–66. https://doi.org/10.1083/jcb.112.2.257 PMID: 1988460

90. Livak KJ, Schmittgen TD. Analysis of relative gene expression data using real-time quantitative PCR and the 2(-Delta Delta C(T)) Method. Methods. 2001;25(4):402–8. https://doi.org/10.1006/meth.2001.1262 PMID: 11846609

91. Persson E, Sonnhammer ELL. InParanoid-DIAMOND: faster orthology analysis with the InParanoid algorithm. Bioinformatics. 2022;38(10):2918–9. https://doi.org/10.1093/bioinformatics/btac194 PMID: 35561192

92. Yu G, He Q-Y. ReactomePA: an R/Bioconductor package for reactome pathway analysis and visualization. Mol Biosyst. 2016;12(2):477–9. https://doi.org/10.1039/c5mb00663e PMID: 26661513

93. Mirdita M, Schütze K, Moriwaki Y, Heo L, Ovchinnikov S, Steinegger M. ColabFold: making protein folding accessible to all. Nat Methods. 2022;19(6):679–82. https://doi.org/10.1038/s41592-022-01488-1 PMID: 35637307

94. Meng EC, Goddard TD, Pettersen EF, Couch GS, Pearson ZJ, Morris JH, et al. UCSF ChimeraX: Tools for structure building and analysis. Protein Sci. 2023;32(11):e4792. https://doi.org/10.1002/pro.4792 PMID: 37774136

95. Blum M, Chang H-Y, Chuguransky S, Grego T, Kandasaamy S, Mitchell A, et al. The InterPro protein families and domains database: 20 years on. Nucleic Acids Res. 2021;49(D1):D344–54. https://doi.org/10.1093/nar/gkaa977 PMID: 33156333

96. Madeira F, Madhusoodanan N, Lee J, Eusebi A, Niewielska A, Tivey ARN, et al. The EMBL-EBI Job Dispatcher sequence analysis tools framework in 2024. Nucleic Acids Res. 2024;52(W1):W521–5. https://doi.org/10.1093/nar/gkae241 PMID: 38597606